ARTICLE IN PRESS

RSE-09141; No of Pages 16

Remote Sensing of Environment xxx (2014) xxx–xxx

Contents lists available at ScienceDirect

Remote Sensing of Environment

journal homepage: www.elsevier.com/locate/rse

Evaluation of the Quasi-Analytical Algorithm for estimating the inherent optical properties of seawater from ocean color: Comparison of Arctic and lower-latitude waters

Guangming Zheng *, Dariusz Stramski, Rick A. Reynolds

Marine Physical Laboratory, Scripps Institution of Oceanography, University of California San Diego, La Jolla, CA 92093–0238, USA

ARTICLE INFO

Article history:
Received 19 June 2013
Received in revised form 2 August 2014
Accepted 4 August 2014
Available online xxxx

Keywords:
Ocean optics
Remote-sensing reflectance
Absorption coefficient
Backscattering coefficient
Inverse reflectance algorithms

ABSTRACT

We evaluated the performance of the Quasi-Analytical Algorithm (QAA, v5 with modifications) for deriving the spectral total absorption, $a(\lambda)$, and backscattering, $b_b(\lambda)$, coefficients of seawater and partitioning of $a(\lambda)$ into phytoplankton and non-phytoplankton components from input spectrum of remote-sensing reflectance, $R_{rs}(\lambda)$, with field data collected in the Arctic and lower-latitude open waters from the Atlantic and Pacific Oceans. The systematic error based on median ratio between QAA-derived and measured $a(\lambda)$ varied from about 1% to $\pm$10% depending on light wavelength and the oceanic region. The QAA typically overestimated $b_b(\lambda)$ from 3% to 14% compared with field measurements. These results were obtained with a correction for Raman-scattering contribution to R_{rs} and separate parameterization of molecular and particulate backscattering in the R_{rs} vs. b_b/a relationship. Without these features the earlier versions of the QAA can overestimate $b_b(\lambda)$ by as much as 35% in clear waters. The use of pure seawater backscattering coefficients accounting for water temperature and salinity improved the accuracy of QAA-derived $a(\lambda)$ in Arctic waters. The absorption-partitioning component of the QAA significantly underestimated phytoplankton absorption and overestimated non-phytoplankton absorption in both Arctic and lower-latitude waters.

1. Introduction

Remote sensing of ocean color is a potentially powerful tool for monitoring critical components of the marine ecosystem, such as the concentrations of colored dissolved organic matter (CDOM) and phytoplankton. However, one of the important prerequisites for utilization of this capability is the availability of appropriate inverse algorithms for estimating the inherent optical properties (IOPs) of seawater and associated seawater constituents from the spectral remote-sensing reflectance of the ocean, $R_{rs}(\lambda)$, where λ represents light wavelength in vacuum. A number of inverse models have been developed and are currently used, including the model of Loisel and Stramski (2000), the Garver-Siegel-Maritorena model (GSM; Maritorena, Siegel, & Peterson, 2002), the Quasi-Analytical Algorithm (QAA; Lee, Carder, & Arnone, 2002), and the model by Smyth, Moore, Hirata, and Aiken (2006). The goal of such models is to determine the IOPs of seawater, including the spectral coefficients for absorption, $a(\lambda)$, and backscattering, $b_b(\lambda)$, from the measured $R_{rs}(\lambda)$.

Although frequently hampered by the availability of adequate datasets, there are ongoing efforts to evaluate the accuracy of such models. One such study conducted by the International Ocean-Colour Coordinating Group (IOCCG, 2006) inter-compared the performance of various inverse models using both in situ and simulated optical datasets. Unfortunately, the in situ dataset used in this study lacked measurements of the backscattering coefficient, which is a key component of all inversion models. Shanmugam, Ahn, Ryu, and Sundarabalan (2010) included field data of both $a(\lambda)$ and $b_b(\lambda)$ in a study evaluating the performance of three inverse models, but the backscattering measurements used were historical and not coincident with absorption measurements in respect to both location and time of data collection. Further efforts to thoroughly evaluate the performance of inverse reflectance models with high-quality in situ data obtained from concurrent measurements of $R_{rs}(\lambda)$, $a(\lambda)$, and $b_b(\lambda)$, are therefore needed.

An additional motivation that emphasizes the need for a more comprehensive model evaluation is that current inverse reflectance algorithms have been typically developed from observations in lower-latitude oceanic waters, but there is a growing demand for applying such models to high-latitude waters such as the Arctic because of ongoing and anticipated changes in the Arctic ecosystem and biogeochemical cycles (e.g., Arrigo et al., 2012; Frey & McClelland, 2009; Li, McLaughlin, Lovejoy, & Carmack, 2009). However, the Arctic waters within the shelf regions are often optically complex with significant inputs of terrigenous CDOM and suspended particles from surrounding rivers (Holmes et al., 2002; Stedmon, Amon, Rinehart, & Walker, 2011), or particulate

* Corresponding author at: NOAA/NESDIS/STAR, NOAA Center for Weather and Climate Prediction (NCWCP), 5830 University Research Court, College Park, MD 20740, USA.
E-mail address: guangming.zheng@noaa.gov (G. Zheng).

http://dx.doi.org/10.1016/j.rse.2014.08.020
0034-4257/

matter originating from shelf resuspension or sediment-laden sea ice (Darby, Myers, Jakobsson, & Rigor, 2011; Nürnberg et al., 1994). As a result, the optical properties of Arctic waters are often quite different from those at lower latitudes (e.g., Matsuoka, Hill, Huot, Babin, & Bricaud, 2011; Matsuoka, Huot, Shimada, & Saitoh, 2007; Mitchell & Holm-Hansen, 1991; Stramska, Stramski, Hapter, Kaczmarek, & Stoń, 2003; Wang & Cota, 2003).

The optical complexity of Arctic waters imposes significant challenges for the development of adequate inverse reflectance algorithms. Wang and Cota (2003) showed that the GSM-derived particulate backscattering coefficient, b_{bp}, at a light wavelength of 443 nm is overestimated by 23% compared with measured data collected in the Chukchi and western Beaufort Seas, while errors in the GSM-derived absorption coefficient of non-phytoplankton materials, a_{dg}, representing the combined contributions of non-algal particles and CDOM to absorption, were even larger. Matsuoka et al. (2007) found that the QAA-derived $a(\lambda)$ correlated well with measured values in the same region, and speculated that model-derived $b_{bp}(\lambda)$ was also likely reasonable in this region. However, field datasets employed in these studies are either small in size or lacking concurrent measurements of other parameters required for a comprehensive analysis. Consequently, conclusions based on the analysis of such limited datasets provide only limited information about the performance of inverse reflectance models and little guidance as regards the actual applicability of these models in Arctic waters.

Recently, a large set of field data with concurrent measurements of IOPs and radiometric quantities that enable determinations of apparent optical properties (AOPs) including the reflectance of the ocean were collected in Arctic waters during three oceanographic cruises; the 2009 MALINA (MAckenzie LIght aNd cArbon) expedition in the southeastern Beaufort Sea (e.g., Matsuoka et al., 2012), and the 2010 and 2011 NASA ICESCAPE (Impacts of Climate on the Eco-Systems and Chemistry of the Arctic Pacific Environment) campaigns in the Chukchi and southwestern Beaufort Seas (Arrigo et al., 2012). The collected data form the largest and most comprehensive bio-optical datasets from the Arctic region to date. In this study, we utilize this dataset to evaluate the performance of both older and recent formulations of the Quasi-Analytical Algorithm (QAA) for this region of the Arctic. For comparison, we also include in our evaluation field data collected during two lower-latitude cruises conducted in the open Pacific and Atlantic Oceans, which provide measurements of the same set of optical variables with similar protocols.

We chose to evaluate the QAA because it is one of the most widely used inverse algorithms for ocean color applications, and is included in the standard codes for processing satellite ocean color data as part of NASA's SeaDAS (SeaWiFS Data Analysis System; Baith, Lindsay, Fu, & McClain, 2001) software. This model derives $a(\lambda)$ and $b_b(\lambda)$ from ocean reflectance measurements, and also includes a capability for partitioning $a(\lambda)$ into phytoplankton, $a_{ph}(\lambda)$, and non-phytoplankton, $a_{dg}(\lambda)$, components. Our analysis focuses on the most recently-published version of QAA (Lee et al., 2013), which is based on the so-called version 5 of the model (v5; Lee, Lubac, Werdell, & Arnone, 2009) but utilizes a modification to the assumed relationship between $R_{rs}(\lambda)$ and IOPs and also incorporates a correction to account for the contribution of Raman scattering to $R_{rs}(\lambda)$ (described in Section 3). We also provide a comparison with the unmodified QAA(v5), which has been utilized in many studies over the past several years. In the evaluation analysis, we quantified errors in the QAA-derived $a(\lambda)$ and $b_b(\lambda)$ and identified and quantified major error sources for the model outputs through sensitivity analysis. We also evaluated the performance of the second part of the QAA that partitions $a(\lambda)$ into $a_{ph}(\lambda)$ and $a_{dg}(\lambda)$ components and compared these results with the performance of a recently developed partitioning model (Zheng & Stramski, 2013). Our findings have important implications for an understanding of the performance of the QAA and potential refinements of this and other inverse models for applications within the world oceans including Arctic waters.

2. Field data of inherent and apparent optical properties

In the present study we used field observations of IOPs and AOPs of the ocean collected in both Arctic and lower-latitude waters. The Arctic data were collected mostly within the shelf areas with a smaller number of data collected in open waters of the Canada basin. The data from lower latitudes were collected mostly in oligotrophic and mesotrophic waters of the eastern South Pacific and eastern Atlantic Oceans. The lower-latitude data also contain measurements obtained at a few stations in eutrophic waters within the coastal upwelling zone off Chile.

The Arctic data were collected during three oceanographic cruises (Fig. 1). In July and August of 2009 the MALINA expedition was conducted onboard the CCGS *Amundsen* in the southeastern Beaufort Sea. In June and July of both 2010 and 2011 the cruises onboard the USCGS *Healy* took place in the Chukchi and southwestern Beaufort Seas as part of the NASA program ICESCAPE. For the MALINA cruise, we excluded from our analyses the data collected at 11 stations in highly turbid waters in the vicinity of the Mackenzie River mouth. The final Arctic dataset consists of 77 stations, which includes 26 stations from MALINA and 51 stations from ICESCAPE. The majority of stations (74 out of 77) provide concurrent determinations of both IOPs and AOPs, including hyperspectral measurements of the absorption coefficients of particulate and colored dissolved organic matter, multispectral measurements of the backscattering coefficient, and multispectral data of the remote-sensing reflectance. This MALINA/ICESCAPE dataset represents the largest set of optical measurements conducted so far in the Arctic Ocean in terms of the number of stations that have concurrent determinations of these optical properties with consistent methodology. This feature of the dataset is particularly important for pursuing our goal of thoroughly evaluating the performance of the QAA.

The lower-latitude data were collected during two cruises; one in open waters of the eastern South Pacific and the other in the eastern Atlantic Ocean. The BIOSOPE expedition in the Pacific was conducted onboard the French R/V *l'Atalante* from October through December, 2004. Details about oceanographic work conducted on this cruise which are most relevant to this study can be found elsewhere (Bricaud, Babin, Claustre, Ras, & Tièche, 2010; Stramski et al., 2008). The ANT-XXIII/1 expedition in the Atlantic was conducted onboard the German R/V *Polarstern* in October and November, 2005 (see Stramski et al., 2008 for relevant details). In total 54 lower-latitude stations were selected for the present study including 30 BIOSOPE stations and 24 ANT-XXIII/1 stations. Concurrent determinations of remote-sensing reflectance, absorption coefficients, and backscattering coefficient are available at 39 of these stations. These data were obtained with similar measurement protocols as the Arctic data.

2.1. Absorption coefficients of seawater constituents

The evaluation of the QAA requires measurements of spectral absorption and backscattering coefficients of surface seawater. Determinations of the spectral absorption coefficients of seawater and its constituents essentially involve direct measurements of three quantities, namely the particulate absorption coefficient, $a_p(\lambda)$, the non-algal particulate (also referred to as detritus) absorption coefficient, $a_d(\lambda)$, and the absorption coefficient of CDOM (also known as gelbstoff or yellow substance), $a_g(\lambda)$. All of the coefficients in this dataset were measured within a broad spectral range extending from 200–300 nm to 735–850 nm with a spectral resolution of 1 nm.

Based on these directly measured quantities, the spectral total absorption coefficient of seawater, $a(\lambda)$, was calculated as the sum of $a_p(\lambda)$, $a_g(\lambda)$, and the absorption coefficient of pure seawater, $a_w(\lambda)$, which is assumed to be known and constant. In our study the values of $a_w(\lambda)$ were taken from the study of Pope and Fry (1997). The phytoplankton absorption coefficient, $a_{ph}(\lambda)$, was calculated by subtracting $a_d(\lambda)$ from $a_p(\lambda)$. The $a_{dg}(\lambda)$ coefficient was calculated as the sum of $a_d(\lambda)$ and $a_g(\lambda)$.

Please cite this article as: Zheng, G., et al., Evaluation of the Quasi-Analytical Algorithm for estimating the inherent optical properties of seawater from ocean color: Comparison of..., *Remote Sensing of Environment* (2014), http://dx.doi.org/10.1016/j.rse.2014.08.020

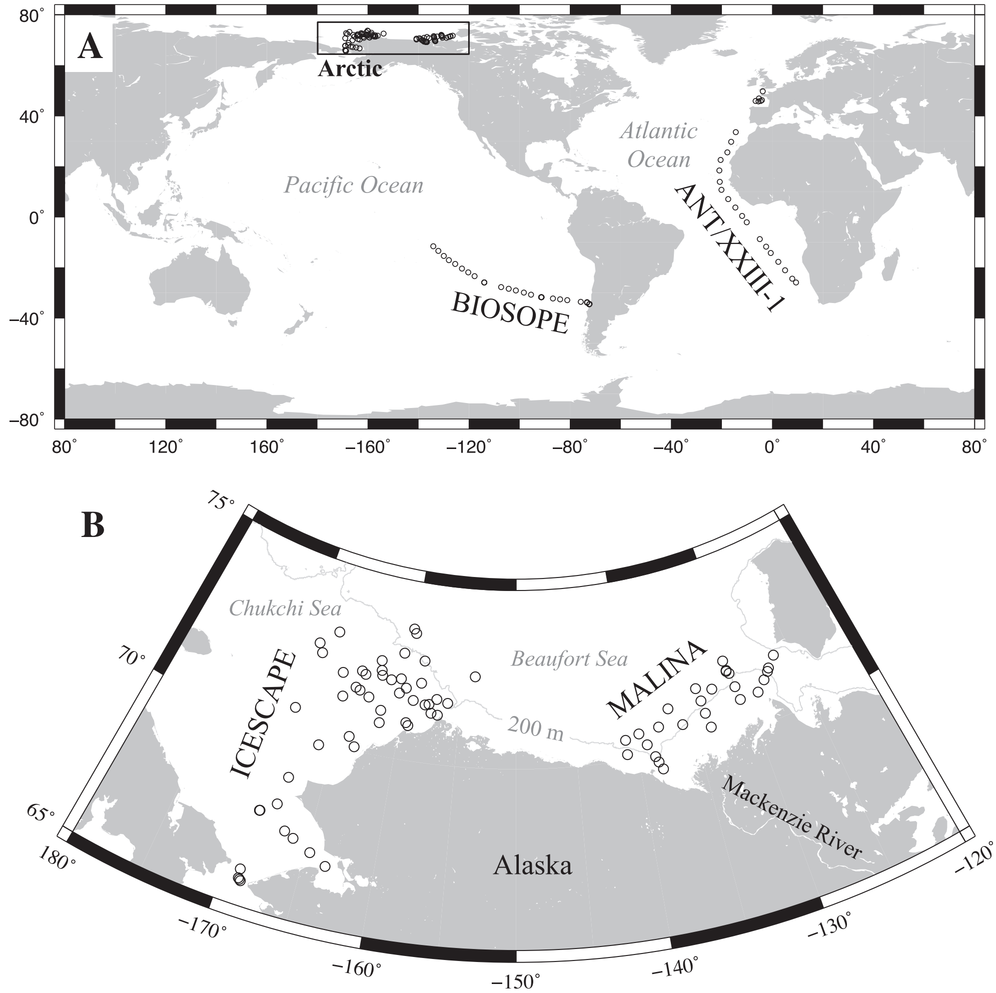

Fig. 1. (A) A global map depicting sampling stations for the MALINA and ICESCAPE cruises (box labeled **Arctic**) conducted in the Arctic, and the BIOSOPE and ANT-XXIII/1 cruises conducted at lower latitudes. (B) Arctic box of panel A enlarged and presented in polar projection. The gray contour lines indicate the 200-m isobath.

On all cruises, spectra of $a_p(\lambda)$ were measured spectrophotometrically on discrete water samples collected with a CTD-Rosette using the quantitative filter-pad technique (e.g., Mitchell, Kahru, Wieland, & Stramska, 2002) but with some methodological differences between the Arctic and lower-latitude cruises. For the MALINA and ICESCAPE cruises, $a_p(\lambda)$ was obtained by measuring the spectral absorbance [i.e., optical density, $OD(\lambda)$] of sample GF/F filters positioned inside an integrating sphere of the spectrophotometer (Perkin-Elmer Lambda 18 equipped with a 15-cm integrating sphere). The inside-sphere configuration is an advancement towards a goal of determining the absorption coefficient of particles with the highest possible accuracy (Babin & Stramski, 2002; Röttgers & Gehnke, 2012). For the lower-latitude cruises, $a_p(\lambda)$ was measured with other variants of the filter-pad technique. Specifically, the transmittance (T) filter-pad technique (e.g., Mitchell, 1990; Mitchell et al., 2002) was used on the BIOSOPE cruise and the transmittance-reflectance (T-R) filter-pad technique (Tassan & Ferrari, 1995, 2002) was used on the ANT-XXIII/1 cruise. Details about methods of $a_p(\lambda)$ measurement for these two cruises can be found in the studies of Bricaud et al. (2010) and Torrecilla, Stramski, Reynolds, Millán-Núñez, and Piera (2011).

To correct the measured spectral optical density, $OD(\lambda)$, of particles retained on the filters for pathlength amplification effect, the same formula was used for all three Arctic cruises. The formula is $OD(\lambda)_{\text{suspension}} = 0.3233\ OD(\lambda)_{\text{filter}}^{1.0877}$, where $OD(\lambda)_{\text{suspension}}$ is the optical density that would be measured if particles were in a hypothetical suspension without being subject to multiple-scattering effects, and $OD(\lambda)_{\text{filter}}$ stands for the measured optical density of particles retained on the filter. This formula was determined from experiments with diverse particle samples in our laboratory, which included phytoplankton cultures, phytoplankton-dominated natural waters, and mineral-dominated waters (data unpublished). The complete formula for converting the measured $OD(\lambda)_{\text{filter}}$ into $a_p(\lambda)$ is: $a_p(\lambda) = \ln(10)\ 0.3233\ OD(\lambda)_{\text{filter}}^{1.0877} / (V/A)$, where V is the filtration volume in m^3 and A is the clearance area of filtration in m^2. Other formulas correcting for the pathlength amplification effect were used for the BIOSOPE (Allali, Bricaud, & Claustre, 1997; Bricaud & Stramski, 1990) and ANT-XXIII/1 (Stramska, Stramski, Kaczmarek, Allison, & Schwarz, 2006) data from lower latitudes, in which different spectrophotometric configurations were used.

Spectra of $a_d(\lambda)$ were measured on the same sample filters as $a_p(\lambda)$ after subjecting the filters to cold methanol extraction (Kishino, Takahashi, Okami, & Ichimura, 1985), except for samples from ANT-XXIII/1 which were bleached with sodium hypochlorite (Ferrari & Tassan, 1999). After measuring the $OD(\lambda)$ values for the non-algal particulate component, spectral smoothing, and conversion to absorption coefficient $a_d(\lambda)$, the spectra of $a_p(\lambda)$ and $a_d(\lambda)$ were further processed by making a near-infrared baseline adjustment. For the Arctic data obtained with inside-sphere measurements, the spectrum of $a_d(\lambda)$ was shifted with an offset to ensure that the average value of measured $a_d(\lambda)$ within the spectral range of 800–820 nm was equal to the average value of corresponding $a_p(\lambda)$ in this spectral range. The spectrum of $a_p(\lambda)$ remained unchanged. For BIOSOPE data obtained with a T-

Please cite this article as: Zheng, G., et al., Evaluation of the Quasi-Analytical Algorithm for estimating the inherent optical properties of seawater from ocean color: Comparison of..., *Remote Sensing of Environment* (2014), http://dx.doi.org/10.1016/j.rse.2014.08.020

technique, the so-called "null-point" correction was applied to both $a_p(\lambda)$ and $a_d(\lambda)$ spectra so that the magnitudes of both spectra in the near-infrared are zero (e.g., Mitchell et al., 2002). For ANT-XXIII/1 data obtained with a T-R technique, the spectrum of $a_d(\lambda)$ was processed in a similar way to the Arctic data, with the exception that the spectral range of 840–850 nm was used as the basis for adjusting the values of $a_d(\lambda)$ so that they equaled $a_p(\lambda)$ at these near-infrared wavelengths.

Spectra of $a_g(\lambda)$ were measured with an UltraPath instrument (World Precision Instruments, Inc.; Bricaud et al., 2010; Matsuoka et al., 2012), except for samples from ANT-XXIII/1 which were measured with a PSICAM instrument (Röttgers & Doerffer, 2007; Röttgers et al., 2005). Both UltraPath and PSICAM instruments provide determinations of $a_g(\lambda)$ with sufficient signal-to-noise ratio for the short-wavelength portion of spectrum (less than 550 nm), which eliminates a need for fitting of the spectrum. At longer wavelengths, however, there are often artifacts in measured $a_g(\lambda)$ which are likely caused by variations in the baseline absorption of pure water. To avoid these experimental imperfections, we fitted the measured spectral values from 400 nm to ~550 nm with an exponential function of wavelength with the sole purpose of adopting the values from the fitted function only for wavelengths longer than ~550 nm. The final spectra of $a_g(\lambda)$ were obtained by merging the original measured spectral values at wavelengths shorter than ~550 nm with the extrapolated values from the fit at longer wavelengths. The exact wavelength where the measured portion of the spectrum was connected with the fitted function varied among the samples, depending on the magnitude of the fitted function relative to the measurement in the vicinity of 550 nm.

2.2. Backscattering coefficient of seawater

The spectral backscattering coefficient of seawater, $b_b(\lambda)$, was measured with in situ instruments deployed in a vertical profiling mode. On the BIOSOPE, ANT-XXIII/1, and MALINA cruises, these determinations were made from measurements with a HydroScat-6 and two a-βeta sensors (HOBI Labs, Inc.). These sensors provide a measurement of the spectral volume scattering function at a scattering angle centered at 140°, $\beta(140°, \lambda)$ (Maffione & Dana, 1997). The HydroScat-6 provided measurements at six wavelengths (nominal wavelengths of 442, 470, 550, 589, 620, and 671 nm) and the a-βeta sensors at one wavelength each (420 and 510 nm). The 620-nm band failed to operate correctly on the BIOSOPE cruise, and the 420-nm band failed on the MALINA cruise. On the two ICESCAPE cruises, the determinations of $b_b(\lambda)$ were made from measurements with two HydroScat-6 instruments. One instrument included the wavelengths centered at 420, 470, 532, 550, 640, and 730 nm, and the other included 394, 442, 510, 550, 589, and 852 nm. The 550-nm band is common for both instruments, and the 442-nm band failed to work properly on the ICESCAPE cruise in 2010.

Calculations of the spectral backscattering coefficient from measured raw data for all five cruises were made with the procedure similar to that described by Stramski et al. (2008). Specifically, the $b_b(\lambda)$ coefficient was calculated from the measured spectral volume scattering function at 140°, $\beta(140°, \lambda)$, using the relation: $b_b(\lambda) = b_{bp}(\lambda) + b_{bw}(\lambda) = 2\pi\chi [\sigma(\lambda)\, \beta(140°, \lambda) - \beta_w(140°, \lambda)] + b_{bw}(\lambda)$, where the non-dimensional parameter χ is chosen to be 1.13 for each wavelength, $\sigma(\lambda)$ is a correction factor for attenuation of light, $b_{bw}(\lambda)$ is the pure seawater backscattering coefficient, and $\beta_w(140°, \lambda)$ is the spectral volume scattering function of pure seawater at 140°.

The required input values of $\beta_w(140°, \lambda)$ and $b_{bw}(\lambda)$ for calculating total $b_b(\lambda)$ were estimated from theoretical formulas that take into account the effects of temperature and salinity on scattering by pure seawater. One set of $b_{bw}(\lambda)$ values was determined from the formulas of Buiteveld, Hakvoort, and Donze (1994) for the actual water temperature T and salinity S using the multiplicative adjustment factor for salinity of $(1 + 0.3S/37)$ (Morel, 1974; Twardowski, Claustre, Freeman, Stramski, & Huot, 2007). These calculations were made using T and S from CTD measurements. In these calculations for the Arctic data the depolarization ratio δ for water molecules was assumed to be 0.039 (Farinato & Rowell, 1976; Jonasz & Fournier, 2007). The lower-latitude data were processed several years ago with $\delta = 0.051$ (Stramski et al., 2008), which is consistent with the original formulas for $b_{bw}(\lambda)$ given by Buiteveld et al. (1994). The $b_{bw}(\lambda)$ values estimated using $\delta = 0.051$ are ~2% higher than those using $\delta = 0.039$ at $T = 21$ °C, which was the average temperature for the lower-latitude samples. The second set of estimates of $b_{bw}(\lambda)$ was determined on the basis of the study by Morel (1974). These values were computed for a water temperature of 20 °C, a salinity of 35–39‰, and a depolarization ratio $\delta = 0.09$. The factor $\sigma(\lambda)$ was calculated from the sum of three components, $a_p(\lambda) + a_g(\lambda) + 0.4b_p(\lambda)$, where $b_p(\lambda)$ is the spectral particulate scattering coefficient. For BIOSOPE and MALINA, the coefficients of $a_p(\lambda)$, $a_g(\lambda)$, and $b_p(\lambda)$ were obtained from measurements with ac-9 instruments (Wetlabs Inc.). For ANT-XXIII/1 and ICESCAPE, $\sigma(\lambda)$ was calculated from the beam attenuation coefficient of particles and CDOM at 660 nm, $c_{pg}(660)$, using a functional relationship parameterized from discrete measurements of $a_p(\lambda)$, $a_g(\lambda)$, and $c_{pg}(\lambda)$.

After calculation of σ-corrected $b_b(\lambda, z)$, the profile data were split into down- and upcasts, inspected for quality, smoothed, and averaged into depth bins (0.5 or 1 m). Because the variation in IOPs or significant fluctuations in the measured signal were often observed at very shallow depths, the data collected at the shallowest depths near the surface were not used in subsequent analysis. Surface values of $b_b(\lambda)$ were determined for each cruise by averaging the data over the depth range of 4–6 m for BIOSOPE and 6–8 m for ANT-XXIII/1. For the Arctic cruises, the depth interval for data averaging was typically 2–3 m in thickness and the depth range varied between 1.5 and 5.5 m depending on where the CTD-Rosette bottles were triggered within the near-surface layer. Such a choice ensured that the depths involved in the determination of surface estimates of $b_b(\lambda)$ were consistent with the near-surface depth of discrete water samples at which the absorption coefficients were measured. Such consistency is particularly important for some stations visited during the Arctic cruises where a strong near-surface gradient in vertical profiles of IOPs was observed.

To obtain $b_b(\lambda)$ at arbitrary wavelengths within the visible spectral region, a power function was fitted to the final spectral data of $b_b(\lambda)$ measured at discrete wavelengths. Similarly, estimates of the spectral slope of $b_{bp}(\lambda)$ were calculated by fitting a power function to the discrete spectral measurements of $b_{bp}(\lambda)$. These regression analyses were performed on $\log_{10}$-transformed data, with data at certain wavelengths excluded from the analyses. Specifically, the 620-nm band on the BIOSOPE, the 420-nm band on the MALINA, and the 442-nm band on the ICESCAPE-2010 cruises were excluded because the instruments failed to work properly at these bands. The 671-nm band was excluded from BIOSOPE, ANT-XXII/1, and MALINA data to avoid potential contamination of the backscattering signal by phytoplankton fluorescence. The data measured simultaneously by two 550-nm sensors on the ICESCAPE cruises were averaged before being used for fitting.

2.3. Radiometric quantities and remote-sensing reflectance

The default input of the QAA model is the spectral remote-sensing reflectance just above the sea surface, $R_{rs}(\lambda)$, which is defined as the ratio of water-leaving radiance from the nadir direction, $L_u(\lambda, z = 0^+) \equiv L_w(\lambda)$, to the downwelling plane irradiance just above the sea surface, $E_d(\lambda, z = 0^+) \equiv E_s(\lambda)$. On the BIOSOPE cruise, $R_{rs}(\lambda)$ was determined from direct shipboard above-water measurements of $E_s(\lambda)$, and underwater measurements of upwelling radiance at a depth of 0.2 m, $L_u(\lambda, z = 0.2$ m), made with a hyperspectral radiometer (HyperPro, Satlantic, Inc.). Measurements were made over the spectral region 380–800 nm at 3.3 nm intervals. Measurements of $L_u(\lambda, z = 0.2$ m) were propagated to just below the sea surface to obtain $L_u(\lambda, z = 0^-)$, using an iterative approach that estimates the spectral diffuse attenuation coefficient for $L_u(\lambda)$ from spectral ratios of measured radiance. Computed values of $L_u(\lambda, z = 0^-)$ were then propagated through the sea surface to obtain the water-leaving radiance, $L_w(\lambda)$, using the relation $L_w(\lambda)/L_u(\lambda, z = 0^-) = 0.54$, which takes into account the effects of Fresnel reflectance and refractive effects on solid angle across the water-air interface.

On the ANT-XXIII/1, MALINA, and ICESCAPE cruises, $R_{rs}(\lambda)$ was determined from measurements of underwater vertical profiles of upwelling radiance, $L_u(\lambda, z)$, and downwelling irradiance, $E_d(\lambda, z)$, with freefall spectroradiometers. On the ANT-XXIII/1 cruise, a SeaWiFS Profiling Multichannel Radiometer (Satlantic, Inc.) was used, which provided 13 spectral bands including 412, 442, 490, 510, 555, and 666 nm which are used in this study. On the MALINA cruise, a Compact-Optical Profiling System (Biospherical Instruments, Inc.) provided measurements at 18 spectral bands including 412, 443, 490, 510 555, and 670 nm. On the ICESCAPE cruises, a Profiling Reflectance Radiometer (Biospherical) was used to measure the vertical radiometric profiles at 18 spectral bands including 412, 443, 490, 510 555, and 665 nm.

The radiometric measurements and data processing were consistent with methods described in NASA protocols (Mueller et al., 2003). Profiles were visually inspected for quality, and the data were binned into depth intervals ranging from 0.1 to 1 m depending on the cruise. A depth range within the upper mixed layer (typically 5–20 m for the ANT-XXIII/1 cruise and 1–7 m for the ICESCAPE cruises) was then selected as a basis for extrapolation of $L_u(\lambda, z)$ and $E_d(\lambda, z)$ to immediately beneath the sea surface using the vertical attenuation coefficients for upwelling radiance, $K_{Lu}(\lambda)$, and downwelling irradiance, $K_d(\lambda)$. The estimates of $L_u(\lambda, z = 0^-)$ and $E_d(\lambda, z = 0^-)$ just beneath the surface were propagated through the surface to yield the above-water estimates of $L_w(\lambda)$ and $E_s(\lambda)$. The effective coefficients for propagating $E_d(\lambda, z = 0^-)$ and $L_u(\lambda, z = 0^-)$ through the water-air interface for the ANT-XXIII/1 and ICESCAPE cruises were: $E_s(\lambda)/E_d(\lambda, z = 0^-) = 1/0.957$ and $L_w(\lambda)/L_u(\lambda, z = 0^-) = 0.5425$. For the MALINA cruise, these coefficients were: $E_s(\lambda)/E_d(\lambda, z = 0^-) = 1/0.97$ and $L_w(\lambda)/L_u(\lambda, z = 0^-) = 0.54$. The latter is the same as that used for BIOSOPE data processing.

In the final step of computations, the spectral remote-sensing reflectance just above the sea surface was obtained as $R_{rs}(\lambda) = L_w(\lambda)/E_s(\lambda)$. With the assumptions for the transmittance coefficients of irradiance and radiance across the sea surface, the relationship between $R_{rs}(\lambda)$ and its counterpart reflectance just below the surface, $r_{rs}(\lambda) \equiv L_u(\lambda, z = 0^-)/E_d(\lambda, z = 0^-)$, is: $R_{rs}(\lambda) = 0.519\, r_{rs}(\lambda)$ for the ANT-XXIII/1 and ICESCAPE cruises, and $R_{rs}(\lambda) = 0.524\, r_{rs}(\lambda)$ for the MALINA cruise. The different factors in these relationships represent choices made by individual investigators who collected and processed the radiometric data. The difference in the final estimates of $R_{rs}(\lambda)$ resulting from the use of values of 0.519 and 0.524 is ~0.9%.

3. Description of the Quasi-Analytical Algorithm

The Quasi-Analytical Algorithm (QAA), originally developed by Lee et al. (2002), is a semi-analytical model that derives IOPs, in particular the spectral absorption, $a(\lambda)$, and backscattering, $b_b(\lambda)$, coefficients of seawater, from spectral remote-sensing reflectance $R_{rs}(\lambda)$. The model has been refined several times in the past (Lee et al., 2007, 2009, 2010, 2013). The present study focuses on the most widely utilized version, v5, of the model (Lee et al., 2009) but with two important modifications recently introduced. The first modification is addition of a correction formula to remove the contribution of Raman scattering to measured $R_{rs}(\lambda)$ (Lee et al., 2013). The second modification replaces the $R_{rs}(\lambda)$–IOP formulation proposed by Gordon (1986) and Gordon et al. (1988) with one parameterizing the molecular and particulate backscattering coefficients separately (Lee et al., 2010). In addition to these two major modifications, the present version also employs a formulation which utilizes the above-water spectrum of $R_{rs}(\lambda)$ directly and omits the conversion to its subsurface counterpart $r_{rs}(\lambda)$ (Lee et al., 2013). Finally, we made another modification to the choice of pure seawater backscattering values of $b_{bw}(\lambda)$ by using the estimates based on the equations of Buiteveld et al. (1994) instead of those from Morel (1974). This modification ensures the consistency between the model-derived values and our field data. Hereafter, we simply refer to this modified version as QAA. A sensitivity analysis examining the influence of these modifications is described in Section 4.2, and in that section to avoid ambiguity we refer to the model explicitly as QAA(v5mRB) where "m" refers to the $R_{rs}(\lambda)$–IOP modification, "R" to the addition of the Raman scattering correction, and "B" to the use of $b_{bw}(\lambda)$ calculated according to Buiteveld et al. (1994) with temperature and salinity adjustments.

A simplified flowchart of the QAA is shown in Fig. 2. It first utilizes the input of measured $R_{rs}(\lambda)$ to obtain Raman-corrected $R_{rs}(\lambda)$ (Lee et al., 2013). Following this correction, the model consists of two main parts: Part I derives the coefficients of total absorption $a(\lambda)$ and total backscattering $b_b(\lambda)$ from $R_{rs}(\lambda)$, and Part II partitions $a(\lambda)$ into phytoplankton, $a_{ph}(\lambda)$, and non-phytoplankton, $a_{dg}(\lambda)$, components. The main purpose of this flowchart is to illustrate the general structure of the QAA and aid in identifying the error sources for output variables. We emphasize that this flowchart is simplified and some calculations in the model are not explicitly illustrated.

We categorized the major variables involved in the QAA into primary-derived variables (PDVs) and secondary-derived variables (SDVs) on the basis of the general scheme of error propagation within the model. The PDVs were defined as variables that are derived directly from $R_{rs}(\lambda)$, while the SDVs are calculated from the PDVs (Fig. 2). As a result, the errors in SDVs are subject to errors in all contributing PDVs located upstream along a sequence of error propagation steps. Considering separately the PDVs and SDVs enabled analysis of different error sources for output variables and identification of model components that may require refinements to improve the performance of the QAA. A description of the sequence of computational steps involved in the two parts of the QAA is presented in Appendix A. These steps are numbered in Fig. 2 to facilitate the analysis of error propagation.

4. Evaluation of the QAA performance

4.1. Comparison of the QAA-derived and measured $a(\lambda)$ and $b_b(\lambda)$

In Part I of the QAA the $a(\lambda)$ and $b_b(\lambda)$ coefficients are derived from $R_{rs}(\lambda)$. For our evaluations, the input to QAA consisted of $R_{rs}(\lambda)$ determined from in situ radiometric measurements at each station (Section 2.3). In addition, to ensure consistency between model-derived and measured field parameters, the same values of $b_{bw}(\lambda)$ used for processing field measurements (Section 2.2) were also utilized in the QAA. Unless otherwise noted, the results presented in this study are obtained by feeding the QAA with input of "Buiteveld" $b_{bw}(\lambda)$ values.

We subsequently made a comparative analysis of the QAA-derived and measured values of $a(\lambda)$ and $b_b(\lambda)$ for both the Arctic and lower-latitude datasets, and illustrate results from this analysis for six example wavelengths that are common on past and current satellite ocean color sensors; namely 412, 443, 490, 510, 555, and 670 nm. Assuming that the differences between the model-derived and measured absorption coefficients can be considered to represent errors of the model, we calculated several error parameters for evaluating model performance. Specifically, the median of the ratio of model-derived to measured values, *MR*, was calculated to provide a measure of overall bias in the modeled data relative to measurements. The mean bias, *MB*, calculated as the average difference between model-derived and measured values provides a dimensional measure of overall bias. Note that whereas the *MR* is based on median statistics and thus insensitive to the presence of extreme values of error, this is not the case for the *MB* based on the mean statistics. The overall degree of agreement between the model and measurements is provided by the median value of the absolute percent difference, *MPD*, between the model-derived and measured data and also by the root mean square deviation (*RMSD*) between these data. The slope of a Model II linear regression (major axis) between

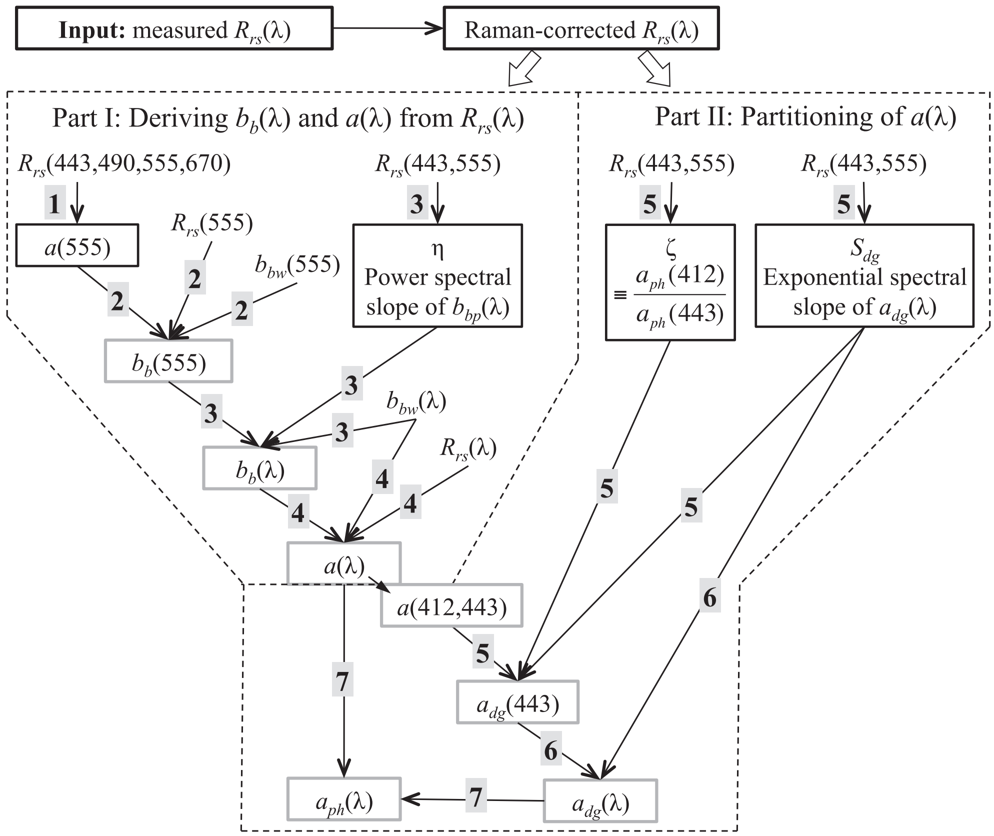

Fig. 2. Simplified flowchart illustrating the modified version 5 of the Quasi-Analytical Algorithm (QAA) used in the present evaluation. Compared with the original version 5 of the model, the present version includes two modifications: 1) correction for Raman scattering effect on spectral remote-sensing reflectance $R_{rs}(\lambda)$; and 2) replacement of the Gordon (1986)-type $R_{rs}(\lambda)$–IOP relationship with Eq. (A1) (see Appendix A). In addition, the conversion from $R_{rs}(\lambda)$ to its underwater counterpart, $r_{rs}(\lambda)$, is omitted in this modified version to be consistent with a more recent publication by Lee et al. (2013). Primary-derived variables calculated directly from $R_{rs}(\lambda)$ are shown in black-edge boxes. Secondary-derived variables computed from primary variables are shown in gray-edge boxes. Numbers 1 through 7 indicate the sequence of computing steps.

model-derived and measured values indicates the degree to which QAA-derived values agree with measurements over the entire dynamic range. Table 1 summarizes these error statistics for both $a(\lambda)$ and $b_b(\lambda)$ at three example wavelengths.

Fig. 3 and Table 1 indicate that for the Arctic cruises, the QAA-derived $a(\lambda)$ agrees well with measurements at the blue and green wavelengths (e.g., 443 and 555 nm), and is poorly correlated with measurements at the red wavelength (670 nm). The best agreement between the QAA-derived and measured values is at the reference wavelength of 555 nm. The systematic component of the error (or bias) expressed in percent, which was calculated from the *MR* of the QAA-derived to measured $a(555)$ as $(MR - 1) \times 100$, is -2.8%. The random component of the error represented by the *MPD* is about 4.3% (Fig. 3E and Table 1). The systematic errors shift towards a more positive bias with a decrease in wavelength from the reference wavelength to shorter wavelengths. For example, the systematic error is $+4.7\%$ for $a(443)$ (Table 1). The random errors also tend to increase towards shorter wavelengths, for example the *MPD* increases to 10.4% for $a(443)$.

At the red wavelength, the QAA-derived and measured $a(670)$ are not well-correlated with a correlation coefficient, *R*, of only 0.48 (Fig. 3F). A significant portion (47%) of model estimates of $a(670)$ are

Table 1
Summary of error statistics for QAA-derived total absorption $a(\lambda)$ and total backscattering $b_b(\lambda)$ coefficients at three example wavelengths for data collected in Arctic waters (MALINA, ICESCAPE) and for data collected in lower-latitude waters (BIOSOPE, ANT-XXIII/1). The *MR* is the median ratio of model-derived to measured values. The *MB* is the mean bias calculated as the average difference between model-derived and measured values. Slope is the linear slope obtained from Model II regression (Pearson's Major Axis) between model-derived and measured values. The *MPD* is the median absolute percent difference calculated as the median of the individual absolute percent differences, $PD_i = 100\,|Y_i - X_i|\,/\,X_i$, where Y_i is the model-derived and X_i is the measured value. The *RMSD* is the root mean square deviation between these data. *N* is the number of observations used for calculating the error statistics.

Variable	Arctic					Lower latitudes				
	MR	*MB* (m^{-1})	Slope	*MPD* (%)	*RMSD* (m^{-1})	*MR*	*MB* (m^{-1})	Slope	*MPD* (%)	*RMSD* (m^{-1})
	$N = 75$					$N = 38$				
$a(443)$	1.047	0.003	1.14	10.44	0.033	0.889	-0.004	0.94	11.53	0.007
$a(555)$	0.972	-0.003	1.04	4.34	0.009	0.977	-0.002	0.92	2.47	0.002
$a(670)$	0.947	-0.023	3.27	12.65	0.080	1.012	0.310	-186.4	27.93	0.546
	$N = 75$					$N = 50$				
$b_b(443)$	1.057	-0.0002	0.69	8.25	0.003	1.137	0.0004	0.91	13.68	0.0005
$b_b(555)$	1.025	-0.0003	0.73	8.62	0.002	1.095	0.0001	0.89	9.82	0.0002
$b_b(670)$	1.048	-0.0001	0.77	11.43	0.002	1.133	0.0001	0.94	13.28	0.0002

Please cite this article as: Zheng, G., et al., Evaluation of the Quasi-Analytical Algorithm for estimating the inherent optical properties of seawater from ocean color: Comparison of..., *Remote Sensing of Environment* (2014), http://dx.doi.org/10.1016/j.rse.2014.08.020

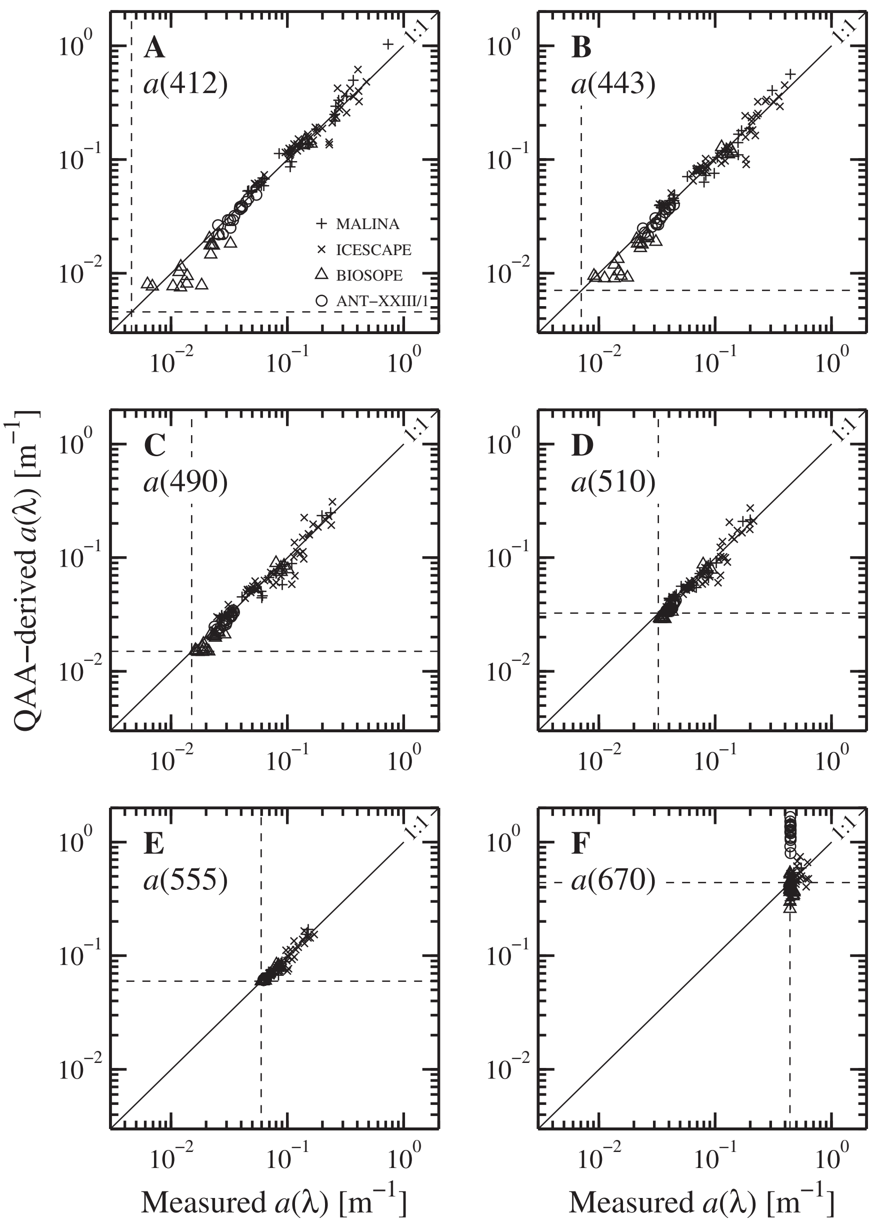

Fig. 3. Comparison between QAA-derived and measured values of total absorption coefficient $a(\lambda)$ for field data collected in Arctic and lower-latitude waters. The dashed lines indicate the magnitude of the pure seawater absorption coefficient $a_w(\lambda)$ at each wavelength. The 1:1 lines are also shown.

lower than the absorption coefficient of pure water. The degree of underestimation is larger than the potential variations in pure water absorption caused by typical environmental changes in water temperature and salinity. Because the ocean reflectance in the red part of the spectrum is generally small due to relatively high absorption coefficient dominated by pure water absorption, even a relatively small error in the measurement of $R_{rs}(670)$ can produce an uncertainty in the derived $a(670)$ such that $a(670) < a_w(670)$. Assuming that the error in model-derived $a(670)$ is produced only by measurement of $R_{rs}(670)$ (which generally is not the case as seen in Fig. 2), we estimated that the maximum tolerable error in $R_{rs}(670)$ ensuring that $a(670) > a_w(670)$ ranges typically from ~1% in clear waters to a few percent in coastal waters. This tolerable error depends on the ratio of non-water to pure water absorption coefficient at this wavelength.

For data obtained at lower latitudes during the BIOSOPE and ANT-XXIII/1 cruises, the QAA-derived $a(\lambda)$ is slightly underestimated at the wavelengths of 412, 443, 490, and 510 nm, agrees well with measurements at 555 nm, and does not correlate with measurements at 670 nm (Fig. 3, Table 1). Little bias was found for the QAA-derived $a(\lambda)$ at 555 nm as the systematic error calculated from the *MR* is only −2.5% (Fig. 3, Table 2). This error increases to around −10% at the wavelengths between 412 and 510 nm. At the red wavelength, the QAA-derived $a(670)$ again exhibits relatively large random errors with the *MPD* increasing to ~28%. There is essentially no correlation ($R = -0.22$) between the QAA-derived and measured absorption coefficients at this wavelength (Fig. 3F). About 44% of the QAA-derived values of $a(670)$ are lower than the pure water absorption, which is almost the same percentage as observed for the Arctic dataset. These results

Table 2
Comparison of performance between the original and four modified versions of QAA(v5). The "v5mRB" represents a modified version with three alternations made to the original model, i.e., "m", "R", and "B", where "m" stands for the replacement of the Gordon (1986) -type $R_{rs}(\lambda)$–IOP relationship with a new one expressed by Eq. (A1) in Appendix A, "R" for the addition of a Raman-correction formula proposed by Lee et al. (2013), and "B" for the use of $b_{bw}(\lambda)$ values calculated according to Buiteveld et al. (1994) and with temperature and salinity adjustments. Similar nomenclature applies to other listed versions "v5mR", "v5R", and "v5m". Note that during the calculations in these three versions the $b_{bw}(\lambda)$ values from Morel (1974) were used.

Variables QAA versions	Arctic		Lower latitudes	
	$(MR-1) \times 100$ (%)	*MPD* (%)	$(MR-1) \times 100$ (%)	*MPD* (%)
***a*(555)**				
v5mRB	−2.8	4.3	−2.3	2.5
v5mR	−2.8	4.2	−2.3	2.5
v5R	−2.7	4.2	−2.2	2.4
v5m	−2.4	3.8	−2.0	2.2
v5	−2.3	3.7	−1.9	2.0
***a*(443)**				
v5mRB	+4.7	10.4	−11.1	11.5
v5mR	+10.9	15.1	−6.9	8.4
v5R	+7.6	12.5	−5.9	7.7
v5m	+11.8	15.8	−4.3	7.4
v5	+8.9	13.2	−2.6	7.4
b_b(555)				
v5mRB	+2.5	8.6	+9.5	9.8
v5mR	+1.7	7.6	+8.4	8.7
v5R	+0.3	9.1	+16.7	16.7
v5m	+6.4	11.8	+20.9	20.9
v5	+4.5	10.9	+26.9	27.0
b_b(443)				
v5mRB	+5.7	8.3	+13.7	13.7
v5mR	+9.5	10.7	+17.6	17.6
v5R	+8.3	12.2	+22.3	22.3
v5m	+13.4	14.7	+26.5	26.5
v5	+11.8	13.8	+30.7	30.7

suggest that the QAA-derived $a(670)$ can be very sensitive to errors in measured reflectance $R_{rs}(670)$.

We conducted a similar comparative analysis with the QAA-derived and measured values of $b_b(\lambda)$ for the field datasets collected in the Arctic and lower-latitude waters. The QAA-derived $b_b(\lambda)$ exhibits good to moderate agreement with measurements at all six examined wavelengths in the spectral region from 412 to 670 nm, as indicated by *MR*-based systematic error ranging from a few percent to less than 20% (Fig. 4 and Table 1). Specifically, for the Arctic cruises, a positive bias of 2.5–8.8% is found for the QAA-derived $b_b(\lambda)$. For data collected from lower latitudes the bias of QAA-derived $b_b(\lambda)$ is somewhat higher ranging from +9.5% to +16.4% within the same spectral range. The systematic errors of QAA-derived $b_b(\lambda)$ is the smallest at the reference wavelength of 555 nm, and increases towards shorter and longer wavelengths. The spectral trend of the *MPD*-based random error is similar to that of the systematic error for the lower-latitude data. For the Arctic data the random error has weak spectral dependence with a small increasing trend from short to long wavelengths.

The Part I of QAA involves the derivation of η, which is a PDV that describes the power spectral slope of $b_{bp}(\lambda)$. It is of interest to know how accurate this variable is because it affects the derivation of $a(\lambda)$ and $b_b(\lambda)$ at non-reference wavelengths. The QAA-derived values of η exhibit relatively high correlation with values derived from measurements (correlation coefficient $R = 0.70$) for the Arctic data, but correlate poorly with measurements ($R = 0.02$) for the lower latitudes (Fig. 5). This result is associated with generally lower particulate contribution to total scattering in the lower latitude waters. The effect of η upon the accuracy of QAA-derived $a(\lambda)$ and $b_b(\lambda)$ is minor for the spectral range between 490 and 670 nm but tends to increase to >5% at wavelengths shorter than 443 nm (not shown).

4.2. Sensitivity analysis of recent modifications to the QAA

The results presented in Section 4.1 are applicable to the most up-to-date description of the QAA, and embed the combined effects of the recent modifications made to the model (see Section 3 and Appendix A). Several studies, however, have used either the unmodified version 5 of the model or some permutation of version 5 incorporating one or more of these modifications (Kahru, Lee, Kudela, Manzano-Sarabia, & Mitchell, 2013; Lee et al., 2010; Mitchell, Cunningham, & McKee, 2014). In addition, in the present study we have replaced the QAA default constant values of $b_{bw}(\lambda)$ obtained from Morel (1974) with values calculated on the basis of Buiteveld et al. (1994) for the sake of consistency with our field measurements. It is therefore of interest to examine the influence of these various modifications on algorithm performance. We determined that the replacement of subsurface $r_{rs}(\lambda)$ with above-water $R_{rs}(\lambda)$ in the parameterization resulted in negligible differences, and omit further discussion of it here. For the other modifications, we conducted a sensitivity analysis to examine impacts of these changes on model performance as compared to field measurements. In this section, we refer to the fully modified version of the model as evaluated in Section 4.1 as the "QAA(v5mRB)", where "m" indicates utilization of the modified $R_{rs}(\lambda)$–IOP formulation, "R" inclusion of the Raman scattering correction, and "B" the use of Buiteveld values of $b_{bw}(\lambda)$. To test the effectiveness of each individual modification to the performance of QAA, we compared key error statistics of selected model outputs calculated using other variants of the model, namely "v5mR", "v5R", "v5m", and the original "v5" (Table 2).

Table 2 indicates that the QAA-derived $a(555)$ is insensitive to changes made in various versions of the model with both error parameters associated with *MR* and *MPD* varying within 1%. For other output variables presented in Table 2 the degree of sensitivity in terms of error statistics varies with geographic regions. For data collected in the Arctic, the model-derived $a(\lambda)$ and $b_b(\lambda)$ are generally insensitive to which version of QAA was used. However, there is a noticeable improvement in QAA-derived $a(443)$ of ~6% when $b_{bw}(\lambda)$ values based on Buiteveld et al. (1994) were used during model implementation, compared with results obtained with $b_{bw}(\lambda)$ estimates from Morel (1974). As seen in Fig. 4, the Morel (1974) estimates of $b_{bw}(\lambda)$ adopted by the QAA are significantly higher than the average values calculated from the Buiteveld et al. (1994) formula for the Arctic field data. This augmentation is on average 20%, 18%, 16%, 15%, 13%, and 9% at the wavelengths of 412, 443, 490, 510, 555, and 670 nm, respectively. These differences are contributed predominantly by the use of different values of δ, and to a lesser extent by the fact that the Arctic surface waters are characterized by lower salinities (14.6 to 32.9‰) and lower temperatures (−1.58 to 8.15 °C) compared with the values used in the Morel (1974) determinations of $b_{bw}(\lambda)$.

For lower-latitude data which were mostly collected in clear waters, the largest difference in model output is observed for the variable $b_b(\lambda)$ derived with different versions of QAA (Table 2). For example, the bias of QAA-derived $b_b(555)$ represented by *MR* is about +8.4% using QAA(v5mR) which includes both the Raman-correction formula and the separate parameterization of molecular and particulate backscattering in the R_{rs}–IOP relationship. In comparison, the same error parameter increases to 20.9% when QAA(v5m) is used, i.e., a version without the Raman-correction, and to 16.7% when QAA(v5R) is used, i.e., a version without the new R_{rs}–IOP relationship. With the original QAA(v5) which does not include the Raman-correction formula and the new R_{rs}–IOP relationship, the QAA-derived $b_b(555)$ is significantly overestimated by as much as 26.9%. These results imply that for clear waters it is essential to correct for the Raman scattering contribution, and to implement the refined parameterization of the R_{rs}–IOP relationship. In this regard the Raman-correction formula proposed by Lee et al. (2013) and the R_{rs}–IOP relationship proposed by Lee et al. (2010), which parameterizes molecular and particulate backscattering coefficient separately, appear to improve the accuracy of QAA-derived $b_b(\lambda)$.

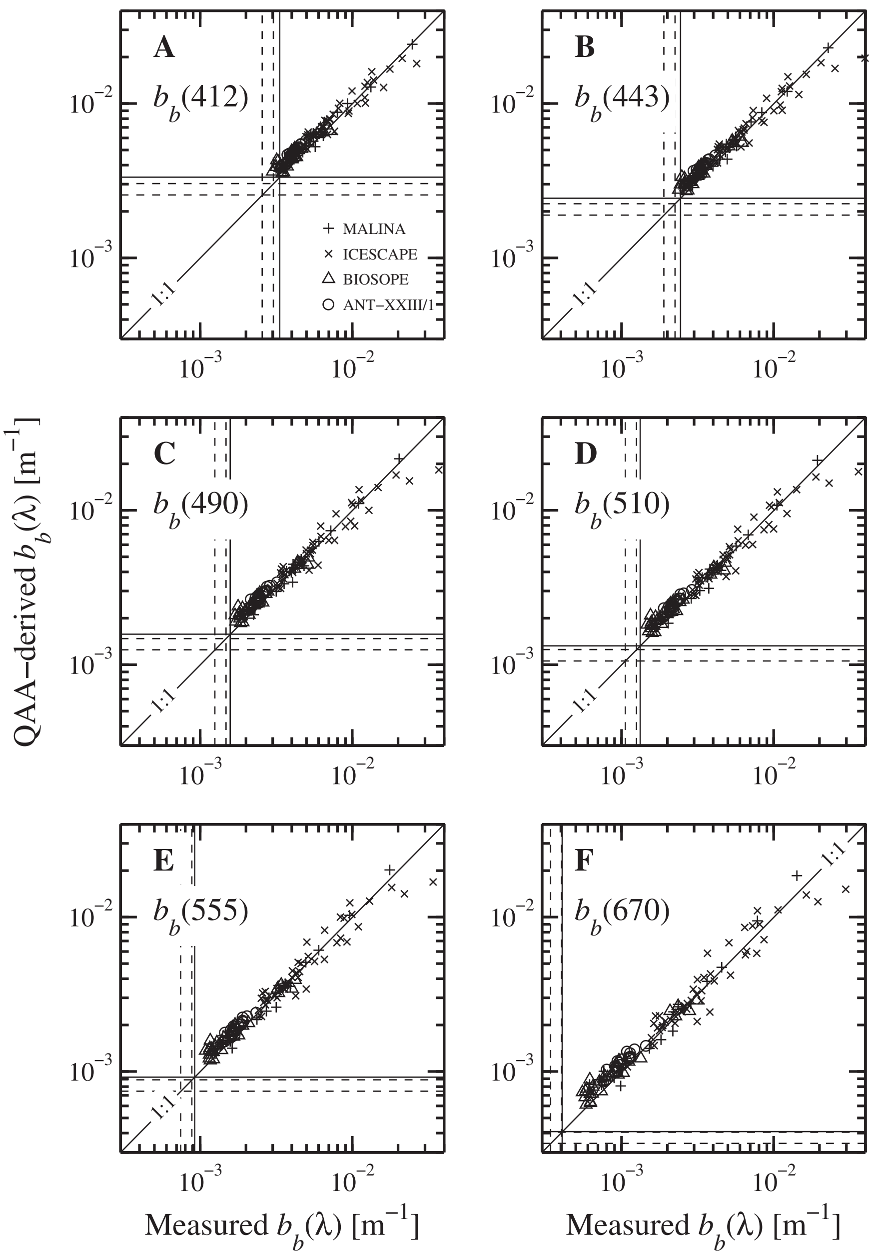

Fig. 4. Similar to Fig. 3 but for total backscattering coefficient $b_b(\lambda)$. Solid horizontal and vertical lines indicate the estimates of the pure seawater backscattering coefficient $b_{bw}(\lambda)$ from Morel (1974). Dashed lines indicate the range of estimates for $b_{bw}(\lambda)$ calculated using the formula from Buiteveld et al. (1994) and adjusted for salinity for both Arctic and lower-latitude data.

It is well-known that the effects of Raman scattering by water molecules are important for ocean reflectance at light wavelengths longer than about 500 nm in clear waters (Gordon, 1999; Morel, Antoine, & Gentili, 2002; Morel & Gentili, 2004). For example, Morel and Gentili (2004) showed that photons originating from Raman scattering can enhance reflectance by at least 15% in the green and red spectral regions for waters with chlorophyll-*a* concentration of 0.03 mg m^{-3}. For a hypothetical ocean containing only pure seawater, the Raman-scattering contribution to water-leaving radiance is between 20–30% for wavelengths longer than 470 nm (Gordon, 1999). Such enhancement of reflectance can cause an overestimation of QAA-derived particulate backscattering coefficient $b_{bp}(\lambda)$ by 50–60%, as reported by Lee et al. (2010) and Westberry, Boss, and Lee (2013) based on data generated with radiative transfer simulations. These findings are consistent with our analysis using data from field measurements, which reveals significant overestimation of $b_b(\lambda)$ and $b_{bp}(\lambda)$ by QAA(v5) for the 60 clearest stations (identified as measured $b_b(555) < 2 \times 10^{-3}$ m^{-1}), including 16 in the Arctic and 44 at lower latitudes. For example, $b_b(555)$ and $b_{bp}(555)$ are overestimated on average by 29.1% and 53.1%, respectively, for these stations (not shown).

Importantly, this is the first time that such significant overestimation of backscattering coefficients in clear waters is demonstrated with evidence based entirely on in situ measurements. Other studies did not reveal this overestimation because either the data used to evaluate the QAA were simulated without inclusion of Raman scattering processes (e.g., IOCCG, 2006), the experimental design was not sufficient to

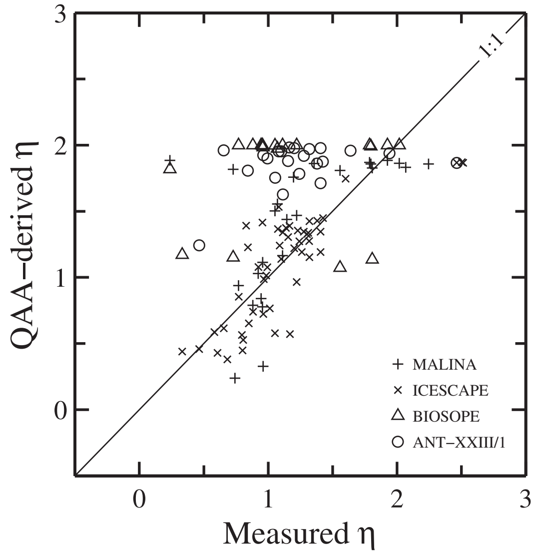

Fig. 5. Comparison between QAA-derived and measured values of the variable η, defined as the power spectral slope of the particulate backscattering coefficient $b_{bp}(\lambda)$.

identify the problem (e.g., Shanmugam et al., 2010), or investigators chose to simply tune the QAA to match in situ measurements (e.g., Kahru et al., 2013). Another important result of our analysis is that no single version of QAA provides the consistently best performance for estimation of both absorption and backscattering coefficients across the range of visible wavelengths and different oceanic regions investigated in this study.

4.3. Comparison of model-derived and measured $a_{dg}(\lambda)$ and $a_{ph}(\lambda)$

The second part of the QAA provides estimates of phytoplankton, $a_{ph}(\lambda)$, and non-phytoplankton, $a_{dg}(\lambda)$, absorption coefficients from inputs of $R_{rs}(443)$, $R_{rs}(555)$, and model-derived $a(\lambda)$. In this section all results are obtained on the basis of QAA(v5mRB). Figs. 6 and 7 illustrate the comparisons between the QAA-derived and measured $a_{dg}(\lambda)$ and $a_{ph}(\lambda)$, respectively, for both Arctic and lower-latitude waters. For the Arctic data, $a_{dg}(\lambda)$ is generally overestimated at short wavelengths (Fig. 6). For example, the bias calculated from the *MR* of the QAA-derived to measured $a_{dg}(\lambda)$ is between +7.5% and +16.7% in the spectral range from 412 to 510 nm. The random error represented by *MPD* is between 11.7% and 24.6% at these wavelengths. Small systematic error is observed for a_{dg} at the reference wavelength of 555 nm. In the red spectral band at 670 nm, $a_{dg}(\lambda)$ is significantly underestimated with a bias of −56.8%. For lower-latitude datasets, the bias of $a_{dg}(\lambda)$ is smaller compared with the Arctic data, and ranges from −11.1% to +1.6%, except for the red band where this systematic error is about −37.4%.

Compared with $a_{dg}(\lambda)$, the errors associated with $a_{ph}(\lambda)$ are much larger (Fig. 7). For the Arctic data, $a_{ph}(\lambda)$ is significantly underestimated at all examined wavelengths except for 670 nm. The systematic error for the QAA-derived $a_{ph}(\lambda)$ is between −52.5% and −101.1% at wavelengths from 412 to 555 nm. A large number of negative values of $a_{ph}(\lambda)$, ranging from 30% to 52% of all examined samples depending on wavelength, was produced by the QAA. This result is consistent with reports of a significant number of negative values of the QAA-derived $a_{ph}(\lambda)$ when applied to satellite ocean color imagery in Arctic regions (e.g., Hirawake, Shinmyo, Fujiwara, & Saitoh, 2012; Zheng, Stramski, & Reynolds, 2010), and indicates the presence of this issue even when no atmospheric correction of $R_{rs}(\lambda)$ is involved. Negative values of $a_{ph}(\lambda)$ were also produced by the QAA for the lower-latitude dataset at wavelengths between 510 and 670 nm.

To identify the main error sources that are responsible for the negative values of $a_{ph}(\lambda)$, we conducted a sensitivity analysis for errors in the QAA-derived $a_{dg}(\lambda)$ and $a_{ph}(\lambda)$. For this analysis we used a "one-factor-at-a-time" approach. Specifically, we ran the QAA model with one model-derived PDV at a time which was considered to contain some error, while keeping all other PDVs at values obtained from field IOP data, which in turn were considered to be error-free. Table 3 depicts example results at the wavelength of 443 nm. For data collected in both the Arctic and lower-latitude waters, the main error sources for the QAA-derived $a_{dg}(443)$ are associated with the parameter η. For lower-latitude waters, additional error comes also from the R_{rs}–IOP relationship at 412 and 443 nm. With respect to the QAA-derived $a_{ph}(443)$ for the Arctic data, the dominant sources of negative bias include the parameters η and S_{dg}, i.e., the relationships that derive these parameters are responsible for the negative values of the QAA-derived $a_{ph}(443)$ in Arctic waters. For lower-latitude data, the bias in the QAA-derived $a_{ph}(443)$ is determined mainly by the interplay between the bias in the R_{rs}–IOP relationship at 555, 412, and 443 nm, which tend to compensate each other. The parameter ζ characterizing the phytoplankton absorption band ratio of $a_{ph}(412)/a_{ph}(443)$, contributes negligible bias to the QAA-derived $a_{ph}(443)$.

The errors in output values of $a_{dg}(\lambda)$ and $a_{ph}(\lambda)$ in Part II of the QAA are also contributed by the errors in the input variable $a(\lambda)$ derived by the model. To evaluate the absorption partitioning by the QAA independently of errors in $a(\lambda)$, we analyzed the performance of Part II of the QAA using the measured values of $a(\lambda)$ as input to this part of the model. This analysis enabled the determination of errors in $a_{dg}(\lambda)$ and $a_{ph}(\lambda)$ resulting solely from the parameterizations involved in Part II of the QAA. For comparison, we also made a similar analysis by applying the same measurements of $a(\lambda)$ [more specifically, the non-water absorption coefficient $a_{nw}(\lambda) = a(\lambda) - a_w(\lambda)$] as input to the absorption partitioning model developed by Zheng and Stramski (2013), hereafter referred to as the stacked-constraints model (SCM). Such comparative analysis of the QAA and the SCM was not feasible for the QAA-derived $a_{nw}(\lambda)$ used as input to the SCM because significant errors associated with the QAA-derived $a_{nw}(\lambda)$ prevented the SCM from finding solutions for the majority of data considered in this study. For example, the random error represented by *MPD* of the QAA-derived $a_{nw}(670)$ is higher than 400% for the MALINA and ICESCAPE data, and higher than 7700% for the BIOSOPE and ANT-XXIII/1 data. The systematic error for the QAA-derived $a_{nw}(510)$ is about −60% for the BIOSOPE and ANT-XXIII/1 data. If the input of $a_{nw}(\lambda)$ is subject to such large errors, the SCM tends to find no solutions. This is mainly because the SCM involves a set of inequality constraints that do not permit unrealistic partitioning results, such as negative values of $a_{ph}(\lambda)$.

One restriction for applying the SCM is for waters containing significant amounts of absorbing mineral particles, for which the spectral shape of absorption spectrum shows considerable departures from an exponential function of wavelength (Zheng & Stramski, 2013; see also Babin & Stramski, 2004; Stramski, Babin, & Woźniak, 2007). Such spectral features violate the assumption of the SCM which requires an exponential spectral shape of $a_{dg}(\lambda)$. We identified 23 MALINA stations and 22 ICESCAPE stations within the Arctic dataset for which the measured spectra of $a_{dg}(\lambda)$ show such non-exponential spectral features indicative of the significant presence of absorbing minerals in water. This is not unexpected as the MALINA and ICESCAPE cruises were conducted mostly within the continental shelf in waters with potential terrestrial influences (Fig. 1). For example, some stations in the Beaufort Sea were located in areas that are subject to influence of terrestrial particulate matter discharged by the Mackenzie River. We excluded these data from the subsequent analysis of absorption partitioning.

Comparisons between model-derived and measured $a_{dg}(443)$ are presented as an example in Fig. 8 for the QAA and the SCM. For brevity, the error statistics are shown only for the combined dataset containing both the Arctic and lower-latitude data (Table 4). For each output

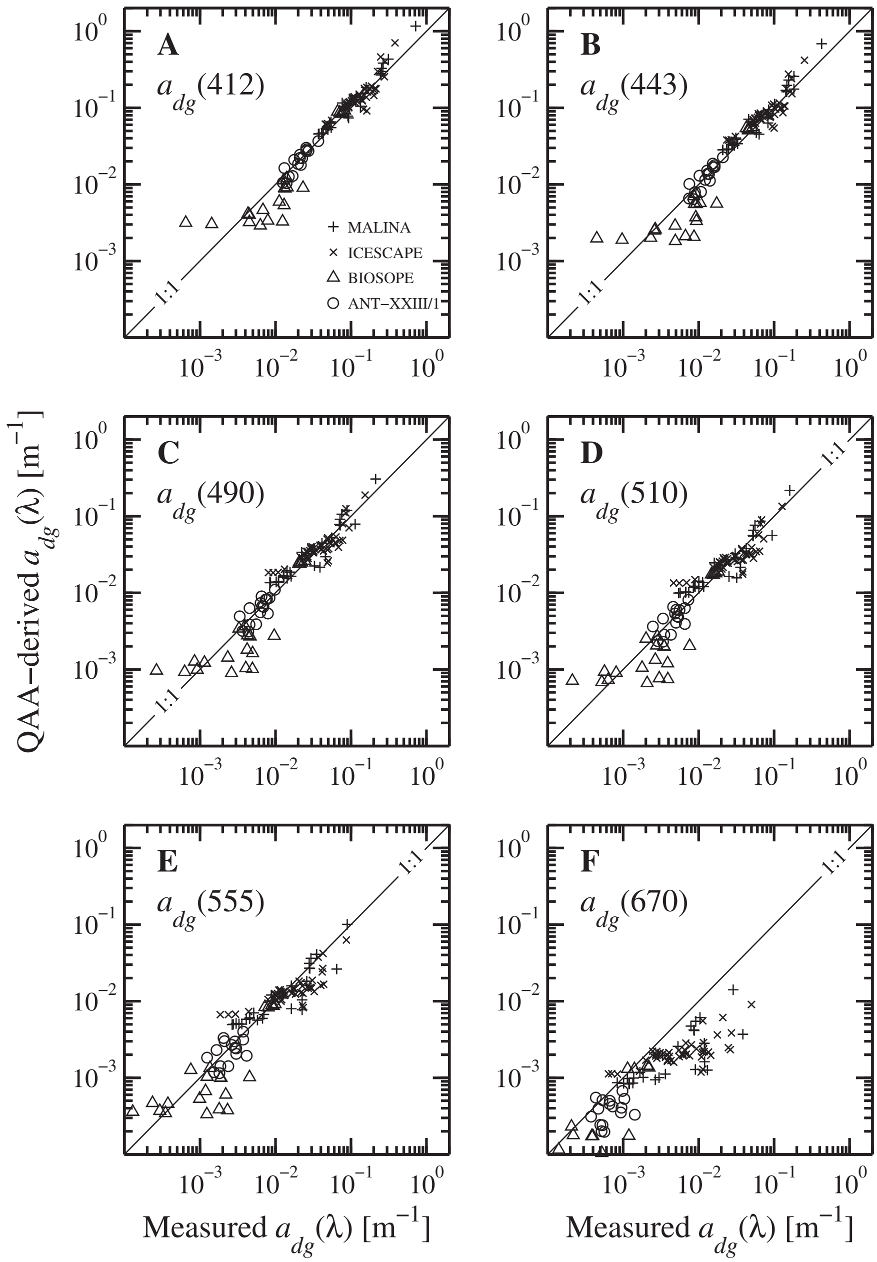

Fig. 6. Comparison of QAA-derived with measured non-phytoplankton (i.e., detritus plus CDOM) absorption coefficient, $a_{dg}(\lambda)$, for field data collected in Arctic and lower-latitude waters. The modeled values were computed using input of measured $R_{rs}(\lambda)$. The 1:1 lines are also shown.

variable of the partitioning model, the SCM provides a range of feasible solutions and also the optimal solution selected from the feasible solutions as the median of all feasible solutions (Zheng & Stramski, 2013). Here we show only the optimal solutions of the SCM. Fig. 8 and Table 4 show that both systematic and random error of the SCM-derived estimates of $a_{dg}(443)$ are smaller than those of the QAA-derived values. The bias of the QAA-derived $a_{dg}(443)$ is +8.5%, in contrast to only −1.4% for the SCM-derived $a_{dg}(443)$. The random error represented by *MPD* of the SCM-derived to measured $a_{dg}(443)$ is 9.1%, compared with 15.9% for the QAA. These reductions in systematic and random errors indicate a better performance of the SCM compared with Part II of the QAA.

Comparisons between the model-derived and measured phytoplankton absorption coefficient, $a_{ph}(443)$, for the QAA and the SCM show results similar to those observed for $a_{dg}(\lambda)$ (Fig. 8 and Table 4). For example, the systematic error for the SCM-derived $a_{ph}(443)$ is about +7.3% and for the QAA-derived values is −12%. The *MPD* for the SCM-derived $a_{ph}(443)$ is 15.1% and for the QAA-derived values is 31.3%. It is also important to note that there is still a significant number of negative values for $a_{ph}(\lambda)$ derived by the QAA even with the input of measured total absorption coefficient $a(\lambda)$ that can be considered to be error-free. We found, for instance, 8 negative QAA estimates of $a_{ph}(443)$ out of 31 measurements in the Arctic waters, and a small number of negative estimates of $a_{ph}(\lambda)$ at 510 and 555 nm for the lower-latitude data.

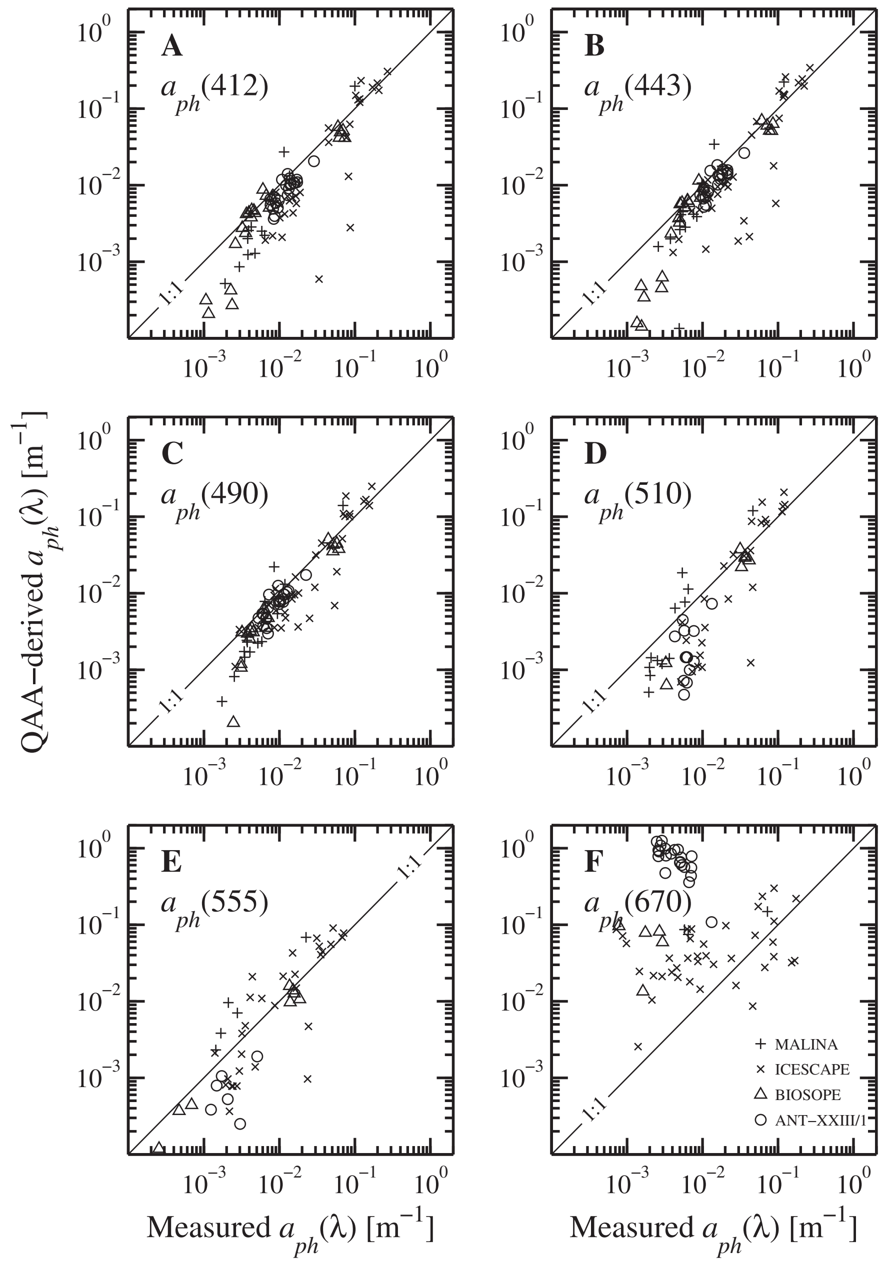

Fig. 7. Similar to Fig. 6 but for the phytoplankton absorption coefficient $a_{ph}(\lambda)$. Note that the negative values of QAA-derived $a_{ph}(\lambda)$, which were determined in 30% to 52% (depending on wavelength) cases out of all Arctic samples, cannot be displayed in this log-log plot. The negative values of QAA-derived $a_{ph}(\lambda)$ between 510 and 670 nm were also determined for the lower-latitude dataset.

Table 3
Contribution of each primary-derived variable to the component bias in secondary-derived variables involved in Part II of QAA. The R_{rs}–IOP relation is defined by Eq. (A1) in the text and η is the power spectral slope of $b_{bp}(\lambda)$. The total number of observations used for determination of error statistics is 75 for the Arctic data and 39 for the lower-latitude data. The parameter ζ is defined as the phytoplankton absorption band ratio $a_{ph}(412)$:$a_{ph}(443)$, and S_{dg} is the exponential spectral slope of $a_{dg}(\lambda)$.

Secondary-derived variables	Total bias (MR−1) × 100 (%)		Component bias (%) contributed by					
			$a(555)$	R_{rs}–IOP relation at 555 nm	η	R_{rs}–IOP relation at 412 and 443 nm	ζ	S_{dg}
$a_{dg}(443)$	Arctic	+16.6	−1.4	+3.3	+12.0	−1.4	+0.1	+2.6
	Lower Latitude	−4.9	−0.4	+1.4	+16.0	−19.7	−0.8	−5.2
$a_{ph}(443)$	Arctic	−52.5	−7.9	+16.3	−24.9	−8.9	−1.2	−12.1
	Lower Latitude	−26.6	−4.0	+20.0	−2.1	−35.0	+0.8	+4.0

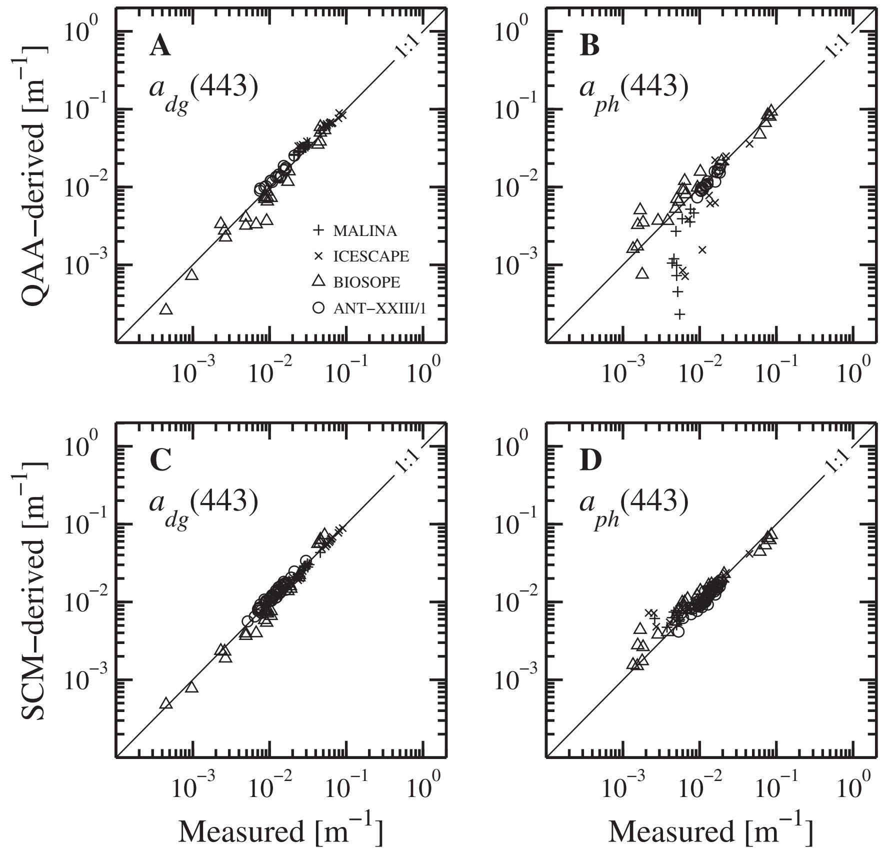

Fig. 8. QAA-derived versus measured $a_{dg}(443)$ (A) and QAA-derived versus measured $a_{ph}(443)$ (B) with input of measured $a(443)$, $R_{rs}(443)$, and $R_{rs}(555)$, for field data collected in Arctic and lower-latitude waters. For comparison, SCM-derived versus measured $a_{dg}(443)$ (C) and SCM-derived versus measured $a_{ph}(443)$ (D) with input of measured $a(443)$ are illustrated. The 1:1 lines are also shown.

5. Conclusions

Our analysis of the performance of the most recent version of the QAA indicates that for blue to green wavelengths the model-derived spectral absorption coefficient, $a(\lambda)$, agrees to within about 10% with in situ measurements obtained from both Arctic and lower-latitude waters. At 670 nm the QAA does not provide robust estimates of the absorption coefficient because of high sensitivity to measurement errors in this spectral region. The QAA-derived backscattering coefficient, $b_b(\lambda)$, generally agrees well with measurements in the Arctic at all examined wavelengths with systematic errors of only a few percent, and is slightly overestimated by ~10% in lower-latitude waters.

The absorption partitioning component of the QAA (i.e., Part II of the model) frequently produces unrealistic negative values of $a_{ph}(\lambda)$, especially for the Arctic data. This issue can potentially be resolved with a new partitioning model, SCM, developed by Zheng and Stramski (2013), which does not yield unrealistic solutions for $a_{dg}(\lambda)$ and $a_{ph}(\lambda)$ and also provides better error statistics at short wavelengths compared with the QAA. These results suggest that replacing Part II of the QAA with the SCM will lead to improved performance of the QAA in terms of estimating $a_{dg}(\lambda)$ and $a_{ph}(\lambda)$. However, it is first important to ensure that the total absorption coefficient of seawater, $a(\lambda)$, is derived with high accuracy from Part I of the QAA. This high accuracy is most critical when the non-water absorption coefficient, $a_{nw}(\lambda)$,

Table 4
Comparison of error statistics between QAA-derived and SCM-derived values of non-phytoplankton, $a_{dg}(\lambda)$, and phytoplankton, $a_{ph}(\lambda)$, absorption coefficients using measured $a(\lambda)$ and $R_{rs}(\lambda)$ as input. The error statistics represent combined results for both Arctic and lower-latitude waters and the total number of observations used for deriving the error statistics is 71, including 31 from the Arctic and 40 from lower latitudes. *MR*, *MB*, *Slope*, *MPD*, and *RMSD* are defined in Table 1.

Model Variable	QAA					SCM				
	MR	*MB* (m^{-1})	*Slope*	*MPD* (%)	*RMSD* (m^{-1})	*MR*	*MB* (m^{-1})	*Slope*	*MPD* (%)	*RMSD* (m^{-1})
$a_{dg}(412)$	1.058	0.003	1.07	9.85	0.005	0.986	0.001	1.05	5.84	0.006
$a_{dg}(443)$	1.086	0.002	1.07	15.56	0.005	0.981	0.0005	1.07	9.09	0.005
$a_{ph}(412)$	0.802	−0.003	0.99	37.40	0.005	1.083	−0.001	0.69	20.35	0.006
$a_{ph}(443)$	0.876	−0.002	1.05	31.93	0.005	1.073	−0.0005	0.78	15.13	0.005

obtained by subtracting the pure water absorption from $a(\lambda)$, makes small contribution to $a(\lambda)$, especially at green wavelengths in clear waters and red wavelengths in most oceanic waters. Therefore, further refinements of Part I of the QAA are desired to provide the best possible estimates of $a(\lambda)$ and $a_{nw}(\lambda)$, which subsequently can be partitioned using the SCM to obtain estimates of $a_{dg}(\lambda)$ and $a_{ph}(\lambda)$.

Our analysis suggests that no single version of QAA provides the consistently best performance for estimation of both absorption and backscattering coefficients across the range of visible wavelengths and different oceanic regions investigated in this study. Nonetheless, in future studies it appears most reasonable to utilize the QAA model with recent modifications that include subtraction of the contribution from Raman scattered photons to measured R_{rs} (Lee et al., 2013) and replacement of the Gordon (1986)-type formulation of the R_{rs}–IOP relationship with one parameterizing the molecular and particulate backscattering coefficients separately (Lee et al., 2010). Without these two modifications the QAA-derived $b_b(\lambda)$ exhibits significant overestimation for clear waters regardless of location, whereas the accuracy of QAA-derived $b_b(\lambda)$ in moderately turbid waters and the accuracy of QAA-derived $a(\lambda)$ for both clear and moderately turbid waters are relatively unaffected.

On the basis of our analysis we also make a recommendation with respect to the choice of $b_{bw}(\lambda)$ values for application of the QAA model in Arctic waters which are characterized by low temperature and relatively low salinity compared with open-ocean lower-latitude waters. The QAA-derived $a(\lambda)$ can also be affected by the choice of $b_{bw}(\lambda)$. Specifically, the use of relatively high default estimates of $b_{bw}(\lambda)$ from Morel (1974) in the QAA model contributes an increase of ~6% in the QAA-derived $a(\lambda)$ at short wavelengths for the Arctic waters compared with the use of more likely lower values of $b_{bw}(\lambda)$. Therefore, in future applications of the QAA in the Arctic waters it will be reasonable to replace the $b_{bw}(\lambda)$ estimates of Morel (1974) with the $b_{bw}(\lambda)$ values calculated with a formula accounting for the actual water temperature and salinity and a value of 0.039 for the depolarization ratio of water molecules (Buiteveld et al., 1994; Jonasz & Fournier, 2007; Stramski et al., 2008; Twardowski et al., 2007; Zhang, Hu, & He, 2009). Such calculations of $b_{bw}(\lambda)$ will require the input data of water temperature and salinity, which can be estimated from satellite observations or climatological data.

Acknowledgments

This work was supported by the NASA Ocean Biology and Biogeochemistry Program (Grants NNG04GO02G and NNX10AG05G), NASA Cryospheric Sciences Program (Grant NNX07AR20G), and the Fred Noel and Sally Spiess Fellowship for graduate students at Scripps Institution of Oceanography. The MALINA project was co-funded by ANR (Agence Nationale de la Recherche), INSU-CNRS (Institut National des Sciences de l'Univers – Centre National de la Recherche Scientifique), CNES (Centre National d'Etudes Spatiales), and ESA (European Space Agency). We thank J. Ehn, S. Kaczmarek, G. Neukermans, M. Stramska, J. Tatarkiewicz, and S. Watanabe for assistance in field data collection and processing. We are grateful to S. Bélanger for providing the MALINA particulate absorption data, S. Hooker for the MALINA radiometric data, A. Matsuoka for the MALINA and ICESCAPE CDOM absorption data, B. G. Mitchell for the ICESCAPE radiometric data, and R. Röttgers for the ANT-XXIII/1 CDOM absorption data. The BIOSOPE absorption and radiometric data were collected by M. Babin, A. Bricaud, H. Claustre, and M. R. Lewis, and were made available to us through the BIOSOPE database. The support of the captains, crew, and fellow scientists onboard the USCCG *Healy*, CCGS *Amundsen*, R/V *l'Atalante*, and R/V *Polarstern* is acknowledged. We thank three reviewers for providing valuable comments.

Appendix A. Calculation steps of the Quasi-Analytical Algorithm used in this study

A.1. Part I of the QAA: Deriving $a(\lambda)$ and $b_b(\lambda)$ from $R_{rs}(\lambda)$

Part I of the QAA utilizes the input of $R_{rs}(\lambda)$ to provide the output of $a(\lambda)$ and $b_b(\lambda)$ (steps 1 through 4 in Fig. 2). This part utilizes a reference wavelength between 550 and 560 nm, with 555 nm chosen in the present study. The PDVs involved in Part I include the total absorption coefficient at the reference wavelength, $a(555)$, and the power spectral slope, η, of particulate backscattering coefficient, $b_{bp}(\lambda)$. It also requires a $R_{rs}(\lambda)$–IOP relationship written as (Lee et al., 2010)

$$R_{rs}(\lambda) = \left(G_0^w + G_1^w \frac{b_{bw}(\lambda)}{a(\lambda)+b_b(\lambda)}\right)\frac{b_{bw}(\lambda)}{a(\lambda)+b_b(\lambda)} + \left(\frac{1}{2}G_0^p + G_1^p \frac{b_{bp}(\lambda)}{a(\lambda)+b_b(\lambda)}\right)\frac{b_{bp}(\lambda)}{a(\lambda)+b_b(\lambda)} \tag{A1}$$

where coefficients G_0^w, G_1^w, G_0^p, and G_1^p are taken as constant values representing averages for various sun-sensor geometries and for a sensor viewing the nadir direction. In the present study these values are 0.0604, 0.0406, 0.0402, 0.1310 sr^{-1}, respectively, and are consistent with those used by Lee et al. (2010), Lee et al. (2011, 2013).

Step 1 derives $a(555)$ from input of $R_{rs}(\lambda)$ at four wavelengths using an empirical nonlinear relationship. Step 2 calculates the backscattering coefficient, $b_b(555)$, from $a(555)$, $b_{bw}(555)$, and $R_{rs}(555)$ based on Eq. (A1). This calculation requires a formula of $b_b(\lambda)$ expressed explicitly as a function of $a(\lambda)$, $b_{bw}(\lambda)$, and $R_{rs}(\lambda)$, which can be obtained by rearranging Eq. (A1)

$$b_b(\lambda) = \left[\sqrt{(C_1(\lambda))^2 - 4C_2(\lambda)C_0(\lambda)} - C_1(\lambda)\right]/(2C_2(\lambda)) \tag{A2}$$

where

$$C_0(\lambda) = (G_1^w + G_1^p)(b_{bw}(\lambda))^2 + (G_0^w - G_0^p)b_{bw}(\lambda)a(\lambda) - R_{rs}(\lambda)(a(\lambda))^2,$$

$$C_1(\lambda) = (G_0^w - G_0^p - 2G_1^p)b_{bw}(\lambda) + (G_0^p - 2R_{rs}(\lambda))a(\lambda), \text{ and}$$

$$C_2(\lambda) = G_0^p + G_1^p - R_{rs}(\lambda).$$

Eq. (A2) was used to derive $b_b(555)$ from $a(555)$ in step 2. Step 3 derives the spectral backscattering coefficient, $b_b(\lambda)$, at the non-reference wavelengths (i.e., for $\lambda \neq 555$ nm) by first subtracting the pure seawater contribution, $b_{bw}(555)$, from $b_b(555)$ to obtain the particulate backscattering coefficient at the reference wavelength, $b_{bp}(555)$. The spectrum of $b_{bp}(\lambda)$ is then calculated through assumption of a power-law spectral shape

$$b_{bp}(\lambda) = b_{bp}(555)\left(\frac{555}{\lambda}\right)^{\eta}, \tag{A3}$$

where η is the spectral slope of $b_{bp}(\lambda)$, which is empirically determined from an exponential function of the blue-to-green reflectance band ratio, $R_{rs}(443)/R_{rs}(555)$. Finally, $b_b(\lambda)$ is calculated as the sum of $b_{bp}(\lambda)$ and $b_{bw}(\lambda)$. The original QAA(v5) adopts the estimates of $b_{bw}(\lambda)$ from Morel (1974). These values are typically different from those used in processing the field measurements of $b_b(\lambda)$, which utilized estimates of $b_{bw}(\lambda)$ based on the equations of Buiteveld et al. (1994). The QAA evaluated in this paper uses the "Buiteveld" $b_{bw}(\lambda)$ values unless otherwise noted, which is consistent with field data. The effects of these differences upon model evaluation are summarized in Section 4.2.

Finally, step 4 derives the spectral absorption coefficient, $a(\lambda)$, at non-reference wavelengths from $b_b(\lambda)$, $b_{bw}(\lambda)$, and $R_{rs}(\lambda)$ using a formula derived from Eq. (A1)

$$a(\lambda) = -b_b(\lambda) + \left[\sqrt{(D_1(\lambda))^2 + 4R_{rs}(\lambda)D_0(\lambda)} + D_1(\lambda)\right]/(2R_{rs}(\lambda)) \quad \text{(A4)}$$

where

$$D_1(\lambda) = G_0^w b_{bw}(\lambda) + G_0^p(b_b(\lambda) - b_{bw}(\lambda)) \text{ and}$$

$$D_0(\lambda) = G_1^w(b_{bw}(\lambda))^2 + G_1^p(b_b(\lambda) - b_{bw}(\lambda))^2.$$

Eq. (A4) was used to derive $a(\lambda)$ from $b_b(\lambda)$ in step 4.

A.2. Part II of the QAA: Partitioning of $a(\lambda)$ into $a_{dg}(\lambda)$ and $a_{ph}(\lambda)$

For studies of many biological and biogeochemical processes in the upper ocean, it is of interest to know the spectral absorption coefficients of phytoplankton, $a_{ph}(\lambda)$, and non-phytoplankton materials, $a_{dg}(\lambda)$. Part II of the QAA was developed to address such needs (steps 5 through 7 in Fig. 2).

Step 5 derives $a_{dg}(443)$, where 443 nm is used as a reference wavelength for deriving the spectral $a_{dg}(\lambda)$ from $a(\lambda)$ at 412 and 443 nm using two new PDVs. These PDVs include ζ that is defined as the phytoplankton absorption band ratio $a_{ph}(412)/a_{ph}(443)$, and S_{dg} which is the exponential spectral slope of $a_{dg}(\lambda)$. The band ratio ζ is parameterized as an empirical relationship involving the blue-to-green band ratio of reflectance, $R_{rs}(443)/R_{rs}(555)$. The spectral slope S_{dg} is derived from another empirical relationship involving $R_{rs}(443)/R_{rs}(555)$. This reflectance ratio is also involved in the derivation of the power spectral slope η of $b_{bp}(\lambda)$ in step 3 and therefore the QAA-derived values of $a_{ph}(412)/a_{ph}(443)$, the exponential spectral slope S_{dg} of $a_{dg}(\lambda)$, and the power spectral slope η of $b_{bp}(\lambda)$ are expected to be correlated.

Step 6 calculates the spectrum of $a_{dg}(\lambda)$ from $a_{dg}(443)$ and the derived slope S_{dg} by assuming an exponential spectral shape. The equation to calculate the spectrum of $a_{dg}(\lambda)$ is written as

$$a_{dg}(\lambda) = a_{dg}(443)\exp\left[-S_{dg}(\lambda - 443)\right]. \quad \text{(A5)}$$

Given the input of the QAA-derived $a(\lambda)$, the accuracy of $a_{dg}(\lambda)$ at all wavelengths is subject to potential errors of $a(555)$, η, ζ, and S_{dg}, as well as errors introduced by Eq. (A1) at the wavelengths of 412, 443, and 555 nm.

Step 7 simply subtracts $a_{dg}(\lambda)$ and $a_w(\lambda)$ from $a(\lambda)$ to obtain the phytoplankton absorption spectrum $a_{ph}(\lambda)$. At the wavelengths of 412, 443, and 555 nm, the potential error sources for $a_{ph}(\lambda)$ are the same as those for $a_{dg}(\lambda)$. At other wavelengths, $a_{ph}(\lambda)$ is also affected by potential errors associated with Eq. (A1).

References

Allali, K., Bricaud, A., & Claustre, H. (1997). Spatial variations in the chlorophyll-specific absorption coefficients of phytoplankton and photosynthetically active pigments in the equatorial Pacific. *Journal of Geophysical Research: Oceans*, *102*, 12,413–12,423.

Arrigo, K. R., Perovich, D. K., Pickart, R. S., Brown, Z. W., van Dijken, G. L., Lowry, K. L., et al. (2012). Massive phytoplankton blooms under Arctic sea ice. *Science*, *336*, 1408.

Babin, M., & Stramski, D. (2002). Light absorption by aquatic particles in the near-infrared spectral region. *Limnology and Oceanography*, *47*, 911–915.

Babin, M., & Stramski, D. (2004). Variations in the mass-specific absorption coefficient of mineral particles suspended in water. *Limnology and Oceanography*, *49*, 756–767.

Baith, K., Lindsay, R., Fu, G., & McClain, C. R. (2001). Data analysis system developed for ocean color satellite sensors. *Eos, Transactions American Geophysical Union*, *82*, 202.

Bricaud, A., Babin, M., Claustre, H., Ras, J., & Tièche, F. (2010). Light absorption properties and absorption budget of Southeast Pacific waters. *Journal of Geophysical Research: Oceans*, *115*(C8), C08009, http://dx.doi.org/10.1029/2009JC005517.

Bricaud, A., & Stramski, D. (1990). Spectral absorption coefficients of living phytoplankton and nonalgal biogenous matter: A comparison between the Peru upwelling area and the Sargasso Sea. *Limnology and Oceanography*, *35*, 562–582.

Buiteveld, H., Hakvoort, J. H. M., & Donze, M. (1994, October). Optical properties of pure water. *Ocean Optics XII* (pp. 174–183). International Society for Optics and Photonics.

Darby, D. A., Myers, W. B., Jakobsson, M., & Rigor, I. (2011). Modern dirty sea ice characteristics and sources: The role of anchor ice. *Journal of Geophysical Research*, *116*, C09008, http://dx.doi.org/10.1029/2010JC006675.

Farinato, R. S., & Rowell, R. L. (1976). New values of the light scattering depolarization and anisotropy of water. *The Journal of Chemical Physics*, *65*, 593–595.

Ferrari, G. M., & Tassan, S. (1999). A method using chemical oxidation to remove light absorption by phytoplankton pigments. *Journal of Phycology*, *35*, 1090–1098.

Frey, K. E., & McClelland, J. W. (2009). Impacts of permafrost degradation on arctic river biogeochemistry. *Hydrological Processes*, *23*, 169–182.

Gordon, H. R. (1986). Ocean color remote sensing: Influence of the particle phase function and the solar zenith angle. *Eos, Transactions American Geophysical Union*, *44*, 1055.

Gordon, H. R. (1999). Contribution of Raman scattering to water-leaving radiance: A reexamination. *Applied Optics*, *38*, 3166–3174.

Gordon, H. R., Brown, O. B., Evans, R. H., Brown, J. W., Smith, R. C., Baker, K. S., et al. (1988). A semianalytic radiance model of ocean color. *Journal of Geophysical Research: Atmospheres*, *93*(D9), 10909–10924.

Hirawake, T., Shinmyo, K., Fujiwara, A., & Saitoh, S. I. (2012). Satellite remote sensing of primary productivity in the Bering and Chukchi Seas using an absorption-based approach. *ICES Journal of Marine Science*, *69*, 1194–1204.

Holmes, R. M., McClelland, J. W., Peterson, B. J., Shiklomanov, I. A., Shiklomanov, A. I., Zhulidov, A. V., et al. (2002). A circumpolar perspective on fluvial sediment flux to the Arctic Ocean. *Global Biogeochemical Cycles*, *16*, 1098.

IOCCG (2006). Remote Sensing of Inherent Optical Properties: Fundamentals, Tests of Algorithms, and Applications. In Z. -P. Lee (Ed.), *Reports of the International Ocean-Colour Coordinating Group, No. 5*. Dartmouth, Canada: IOCCG.

Jonasz, M., & Fournier, G. R. (2007). *Light Scattering by Particles in Water, Theoretical and Experimental Foundations.* Amsterdam: Elsevier, 704.

Kahru, M., Lee, Z., Kudela, R. M., Manzano-Sarabia, M., & Mitchell, B. G. (2013). Multi-satellite time series of inherent optical properties in the California Current. *Deep-Sea Research Part II*, http://dx.doi.org/10.1016/j.dsr2.2013.07.023.

Kishino, M., Takahashi, M., Okami, N., & Ichimura, S. (1985). Estimation of the spectral absorption coefficients of phytoplankton in the sea. *Bulletin of Marine Science*, *37*, 634–642.

Lee, Z. P., Carder, K. L., & Arnone, R. A. (2002). Deriving inherent optical properties from water color: A multiband quasi-analytical algorithm for optically deep waters. *Applied Optics*, *41*, 5755–5772.

Lee, Z. P., Du, K., Voss, K. J., Zibordi, G., Lubac, B., Arnone, R., et al. (2011). An inherent-optical-property-centered approach to correct the angular effects in water-leaving radiance. *Applied Optics*, *50*, 3155–3167.

Lee, Z. P., Hu, C., Shang, S., Du, K., Lewis, M., Arnone, R., et al. (2013). Penetration of UV-visible solar radiation in the global oceans: Insights from ocean color remote sensing. *Journal of Geophysical Research: Oceans*, *118*, 4241–4255.

Lee, Z. P., Lubac, B., Werdell, J., & Arnone, R. (2009). An update of the quasi-analytical algorithm (QAA_v5). *IOCCG software report* (http://www.ioccg.org/groups/Software_OCA/QAA_v5.pdf).

Lee, Z. P., Shang, S., Hu, C., Lewis, M., Arnone, R., Li, R., et al. (2010). Time series of bio-optical properties in a subtropical gyre: Implications for the evaluation of interannual trends of biogeochemical properties. *Journal of Geophysical Research*, *115*, C09012, http://dx.doi.org/10.1029/2009JC005865.

Lee, Z. P., Weidemann, A., Kindle, J., Arnone, R., Carder, K. L., & Davis, C. (2007). Euphotic zone depth: Its derivation and implication to ocean-color remote sensing. *Journal of Geophysical Research: Oceans*, *112*, C03009, http://dx.doi.org/10.1029/2006JC003802.

Li, W. K., McLaughlin, F. A., Lovejoy, C., & Carmack, E. C. (2009). Smallest algae thrive as the Arctic Ocean freshens. *Science*, *326*, 539.

Loisel, H., & Stramski, D. (2000). Estimation of the inherent optical properties of natural waters from irradiance attenuation coefficient and reflectance in the presence of Raman scattering. *Applied Optics*, *39*, 3001–3011.

Maffione, R. A., & Dana, D. R. (1997). Instruments and methods for measuring the backward scattering coefficient of ocean waters. *Applied Optics*, *36*, 6057–6067.

Maritorena, S., Siegel, D., & Peterson, A. (2002). Optimization of a semi-analytical ocean color model for global-scale applications. *Applied Optics*, *41*, 2705–2714.

Matsuoka, A., Hill, V., Huot, Y., Babin, M., & Bricaud, A. (2011). Seasonal variability in the light absorption properties of western Arctic waters: Parameterization of the individual components of absorption for ocean color applications. *Journal of Geophysical Research: Oceans*, *116*, C02007, http://dx.doi.org/10.1029/2009JC005594.

Matsuoka, A., Huot, Y., Shimada, K., & Saitoh, S. I. (2007). Bio-optical characteristics of the Western Arctic Ocean: Implications for ocean color algorithms. *Canadian Journal of Remote Sensing*, *33*, 503–518.

Matsuoka, A., Bricaud, A., Benner, R., Para, J., Sempéré, R., Prieur, L., et al. (2012). Tracing the transport of colored dissolved organic matter in water masses of the Southern Beaufort Sea: Relationship with hydrographic characteristics. *Biogeosciences*, *9*, 925–940.

Mitchell, B. G. (1990). Algorithms for determining the absorption coefficient of aquatic particulates using the quantitative filter technique (QFT). *Proceedings of SPIE*, *1302*, 137–148.

Mitchell, B. G., & Holm-Hansen, O. (1991). Bio-optical properties of Antarctic Peninsula waters: Differentiation from temperate ocean models. *Deep Sea Research Part I: Oceanographic Research Papers*, *38*, 1009–1028.

Mitchell, B. G., Kahru, M., Wieland, J., & Stramska, M. (2002). Determination of spectral absorption coefficients of particles, dissolvedmaterial and phytoplankton for discrete water samples. In J. L. Mueller, & G. S. Fargion (Eds.), *Ocean Optics Protocols for Satellite*

Ocean Color Sensor Validation, Revision 3, Vol. 2. (pp. 231–257). Greenbelt, Maryland: NASA Goddard Space Center.

Mitchell, C., Cunningham, A., & McKee, D. (2014). Remote sensing of shelf sea optical properties: Evaluation of a quasi-analytical approach for the Irish Sea. *Remote Sensing of Environment*, *143*, 142–153.

Morel, A. (1974). Optical properties of pure water and pure seawater. In N. G. Jerlov, & E. S. Nielson (Eds.), *Optical Aspects of Oceanography* (pp. 1–24). San Diego: Academic.

Morel, A., Antoine, D., & Gentili, B. (2002). Bidirectional reflectance of oceanic waters: Accounting for Raman emission and varying particle scattering phase function. *Applied Optics*, *41*, 6289–6306.

Morel, A., & Gentili, B. (2004). Radiation transport within oceanic (case 1) water. *Journal of Geophysical Research: Oceans*, *109*, C06008, http://dx.doi.org/10.1029/2003JC002259.

Mueller, J. L., Morel, A., Frouin, R., Davis, C., Arnone, R., Carder, K., et al. (2003). Radiometric measurements and data analysis protocols. In J. L. Mueller, G. S. Fargion, & C. R. McClain (Eds.), *Optics Protocols for Satellite Ocean Color Sensor Validation, Revision 4. NASA Technical Memorandum 2003-21621, Vol. 3*. (pp. 1–78). Greenbelt, Maryland: NASA Goddard Space Center.

Nürnberg, D., Wollenburg, I., Dethleff, D., Eicken, H., Kassens, H., Letzig, T., et al. (1994). Sediments in Arctic sea ice — implications for entrainment, transport and release. *Marine Geology*, *119*, 185–214.

Pope, R. M., & Fry, E. S. (1997). Absorption spectrum (380–700 nm) of pure water, II, Integrating cavity measurements. *Applied Optics*, *36*, 8710–8723.

Röttgers, R., & Doerffer, R. (2007). Measurements of optical absorption by chromophoric dissolved organic matter using a point-source integrating-cavity absorption meter. *Limnology and Oceanography: Methods*, *5*, 126–135.

Röttgers, R., & Gehnke, S. (2012). Measurement of light absorption by aquatic particles: Improvement of the quantitative filter technique by use of an integrating sphere approach. *Applied Optics*, *51*, 1336–1351.

Röttgers, R., Schönfeld, W., Kipp, P. -R., & Doerffer, R. (2005). Practical test of a point-source integrating cavity absorption meter: The performance of different collector assemblies. *Applied Optics*, *44*, 5549–5560.

Shanmugam, P., Ahn, Y. -H., Ryu, J. -H., & Sundarabalan, B. (2010). An evaluation of inversion models for retrieval of inherent optical properties from ocean color in coastal and open sea waters around Korea. *Journal of Oceanography*, *66*, 815–830.

Smyth, T. J., Moore, G. F., Hirata, T., & Aiken, J. (2006). Semianalytical model for the derivation of ocean color inherent optical properties: Description, implementation, and performance assessment. *Applied Optics*, *45*, 8116–8131.

Stedmon, C. A., Amon, R. M. W., Rinehart, A. J., & Walker, S. A. (2011). The supply and characteristics of colored dissolved organic matter (CDOM) in the Arctic Ocean: Pan Arctic trends and differences. *Marine Chemistry*, *124*, 108–118.

Stramska, M., Stramski, D., Hapter, R., Kaczmarek, S., & Stoń, J. (2003). Bio-optical relationships and ocean color algorithms for the north polar region of the Atlantic. *Journal of Geophysical Research: Oceans*, *108*(C5), 3143, http://dx.doi.org/10.1029/2001JC001195.

Stramska, M., Stramski, D., Kaczmarek, S., Allison, D. B., & Schwarz, J. (2006). Seasonal and regional differentiation of bio-optical properties within the north polar Atlantic. *Journal of Geophysical Research: Oceans*, *111*, C08003, http://dx.doi.org/10.1029/2005JC003293.

Stramski, D., Babin, M., & Woźniak, S. B. (2007). Variations in the optical properties of terrigenous mineral-rich particulate matter suspended in seawater. *Limnology and Oceanography*, *52*, 2418–2433.

Stramski, D., Reynolds, R. A., Babin, M., Kaczmarek, S., Lewis, M. R., Röttgers, R., et al. (2008). Relationships between the surface concentration of particulate organic carbon and optical properties in the eastern South Pacific and eastern Atlantic Oceans. *Biogeosciences*, *5*, 171–201.

Tassan, S., & Ferrari, G. M. (1995). An alternative approach to absorption measurements of aquatic particles retained on filters. *Limnology and Oceanography*, *40*, 1358–1368.

Tassan, S., & Ferrari, G. M. (2002). A sensitivity analysis of the 'Transmittance-Reflectance' method for measuring light absorption by aquatic particles. *Journal of Plankton Research*, *24*, 757–774.

Torrecilla, E., Stramski, D., Reynolds, R. A., Millán-Núñez, E., & Piera, J. (2011). Cluster analysis of hyperspectral optical data for discriminating phytoplankton pigment assemblages in the open ocean. *Remote Sensing of Environment*, *115*, 2578–2593.

Twardowski, M. S., Claustre, H., Freeman, S. A., Stramski, D., & Huot, Y. (2007). Optical backscattering properties of the "clearest" natural waters. *Biogeosciences*, *4*, 1041–1058.

Wang, J., & Cota, G. F. (2003). Remote-sensing reflectance in the Beaufort and Chukchi Seas: Observations and models. *Applied Optics*, *42*, 2754–2765.

Westberry, T. K., Boss, E., & Lee, Z. (2013). Influence of Raman scattering on ocean color inversion models. *Applied Optics*, *52*, 5552–5561.

Zhang, X., Hu, L., & He, M. -X. (2009). Scattering by pure seawater: Effect of salinity. *Optics Express*, *17*, 5698–5710.

Zheng, G., & Stramski, D. (2013). A model based on stacked-constraints approach for partitioning the light absorption coefficient of seawater into phytoplankton and non-phytoplankton components. *Journal of Geophysical Research: Oceans*, *118*, 2155–2174.

Zheng, G., Stramski, D., & Reynolds, R. A. (2010). Evaluation of the QAA Algorithm for Estimating the Inherent Optical Properties from Remote-Sensing Reflectance in Arctic Waters. *Poster presented at 2010 AGU Ocean Sciences Meeting, Portland, Oregon*.

Please cite this article as: Zheng, G., et al., Evaluation of the Quasi-Analytical Algorithm for estimating the inherent optical properties of seawater from ocean color: Comparison of..., *Remote Sensing of Environment* (2014), http://dx.doi.org/10.1016/j.rse.2014.08.020